Revista Mexicana de Astronomía y Astrofísica Revista mexicana de astronomía y astrofísica

ISSN: 0185-1101

Universidad Nacional Autónoma de México, Instituto de Astronomía

Yontan, Talar; Çakmak, Hikmet; Bilir, Selçuk; Banks, Timothy; Raúl, Michel; Canbay, Remziye; Koç, Seliz; Taşdemir, Seval; Erçay, Hülya; Öztürk, Burçin Tanık; Dursun, Deniz Cennet

A Study of The NGC 1193 and NGC 1798 Open Clusters
Using CCD UBV Photometric and Gaia EDR3 Data

Revista mexicana de astronomía y astrofísica, vol. 58, no. 2, 2022, pp. 333-353
Universidad Nacional Autónoma de México, Instituto de Astronomía

DOI: https://doi.org/10.22201/ia.01851101p.2022.58.02.14

Available in: https://www.redalyc.org/articulo.oa?id=57175502014



Complete issue

More information about this article

Journal's webpage in redalyc.org



Scientific Information System Redalyc

Network of Scientific Journals from Latin America and the Caribbean, Spain and Portugal

Project academic non-profit, developed under the open access initiative

# A STUDY OF THE NGC 1193 AND NGC 1798 OPEN CLUSTERS USING CCD UBV PHOTOMETRIC AND GAIA EDR3 DATA

Talar Yontan<sup>1</sup>, Hikmet Çakmak<sup>1</sup>, Selçuk Bilir<sup>1</sup>, Timothy Banks<sup>2,3</sup>, Michel Raúl<sup>4</sup>, Remziye Canbay<sup>5</sup>, Seliz Koç<sup>5</sup>, Seval Taşdemir<sup>5</sup>, Hülya Erçay<sup>5</sup>, Burçin Tanık Öztürk<sup>5</sup>, and Deniz Cennet Dursun<sup>5</sup>

Received June 1 2022; accepted July 14 2022

#### ABSTRACT

We present photometric, astrometric, and kinematic studies of the old open star clusters NGC 1193 and NGC 1798. Both of the clusters are investigated by combining data sets from Gaia Early Data Release 3 (EDR3) and CCD UBV observational data. E(B-V) color excesses are derived for NGC 1193 as  $0.150\pm0.037$  and for NGC 1798 as  $0.505\pm0.100$  mag through the use of two-color diagrams. Photometric metallicities are also determined from two-color diagrams with the results of  $[Fe/H]=-0.30\pm0.06$  dex for NGC 1193 and  $[Fe/H]=-0.20\pm0.07$  dex for NGC 1798. The isochrone fitting distance and age of NGC 1193 are  $5562\pm381$  pc and  $4.6\pm1$  Gyr, respectively. For NGC 1798, these parameters are  $4451\pm728$  pc and  $1.3\pm0.2$  Gyr. Kinematic and dynamic orbital calculations indicate that NGC 1193 and NGC 1798 belong to the thick-disk and thin-disk populations, respectively.

#### RESUMEN

Presentamos un estudio fotométrico, astrométrico y cinemático de los cúmulos abiertos viejos NGC 1193 y NGC 1798. Ambos cúmulos se estudian combinando datos de Gaia Early Data Release 3 (EDR3) con datos CCD UBV. Mediante el uso de diagramas de dos colores se obtienen excesos de color E(B-V) para NGC 1193 de  $0.150\pm0.037$  mag, y para NGC 1798 de  $0.505\pm0.100$  mag. Se determinan las metalicidades fotométricas con los mismos diagramas, y resultan ser de  $[{\rm Fe/H}] = -0.30\pm0.06$  dex para NGC 1193 y de  $[{\rm Fe/H}] = -0.20\pm0.07$  dex para NGC 1798. La distancia y la edad obtenidas con el ajuste de isocronas para NGC 1193 son de  $5562\pm381$  pc y  $4.6\pm1$  giga-años, respectivamente. Para NCG 1798 estos parámetros tienen valores de  $4451\pm728$  pc y  $1.3\pm0.2$  giga-años, respectivamente. Los cálculos cinemáticos y orbitales indican que NGC 1183 pertenece a la población de disco grueso y NGC 1798 a la de disco delgado.

Key Words: open cluster and associations: individual: NGC 1193, NGC 1798 — Galaxy: disc — Hertzsprung-Russell and colour-magnitude

#### 1. GENERAL

Open clusters are identified as groupings of stars, beyond those found in a single multiple star system, that are bound together by their weak self-gravitational forces. As cluster stars are formed by the collapse of the same molecular cloud, their basic astrophysical parameters, such as color excess, dis-

tance, metal abundance, and age are similar while their masses and luminosities can range widely. This paper concentrates on open star clusters inside our own galaxy's disk, which are often called 'galactic clusters'. These properties make such open clusters important tools to investigate the structure, formation, and evolution of the Galactic disk, as well as to give opportunities to enhance our understanding of stellar evolution models. In particular, the study of old open clusters can give insight into the kinematic properties and chemical structure of the Galactic disk (Friel 1995).

 $<sup>^{1}\</sup>mathrm{Department}$  of Astronomy & Space Sciences, Istanbul University, Istanbul, Turkey.

<sup>&</sup>lt;sup>2</sup>Nielsen, Chicago, USA.

<sup>&</sup>lt;sup>3</sup>Harper College, Illinois, USA.

<sup>&</sup>lt;sup>4</sup>Observatorio Astronómico Nacional, Universidad Nacional Autónoma de México, Ensenada, México.

<sup>&</sup>lt;sup>5</sup>Institute of Graduate Studies in Science, Istanbul University, Istanbul, Turkey.

#### 1.1. NGC 1193

In 1786 William Herschel discovered the open cluster NGC 1193 ( $\alpha = 03^{\rm h} 05^{\rm m} 56^{\rm s}.64$ ,  $\delta = +44^{\circ} 22^{'} 58^{''}.80, l = 146^{\circ}.8143, b = -12^{\circ}.1624),$ located in the constellation of Perseus (Drever 1888). Together with an angular size of 2', NGC 1193 has a dense central stellar concentration and is classified as II3m (Ruprecht 1966). King (1962) reported that NGC 1193 is likely to be old. In the study of Janes & Adler (1982), NGC 1193 was identified as a dense, poorly studied open cluster with an angular diameter of 2'. Kaluzny (1988) presented the first CCD BV photometric study of NGC 1193, identifying five possible blue straggler stars in the cluster. By BV isochrone fitting to the color magnitude diagram (CMD), they determined the color excess and distance to be 0.12  $\leq$  E(B-V)  $\leq$  0.23 mag and 4.2 < d < 4.9 kpc, respectively. Additionally the metallicity, distance module, and age of the cluster were adopted as Z = 0.01,  $(m - M)_V = 13.8$  mag, and  $t = 8 \times 10^9$  years. Through investigation of the cluster's color-magnitude diagram, Kaluzny (1988) indicated that subgiant branch stars are more populous than red giant branch stars. Utilizing spectroscopic observations, Friel, Liu, & Janes (1989) calculated the first radial velocity estimate for the cluster as  $\langle V_r \rangle = -82 \text{ km s}^{-1}$ . Friel & Janes (1993) performed medium resolution spectroscopic analyses and estimated the cluster metallicity as [Fe/H] =  $-0.50 \pm 0.18$  dex from four giant members. They also calculated the radial velocities of stars whose values lie within  $-64 \le V_r \le -103 \text{ km s}^{-1}$ . Tadross (2005) used photometric data of Kaluzny (1988) and astrometric data from the USNO-B1.0 catalog of Monet et al. (2003) to determine the cluster's color excess  $E(B-V) = 0.10 \pm 0.06$ , distance modulus  $\mu = 13.90 \pm 0.10$  mag, distance  $d = 5.25 \pm 0.24$  kpc, age t = 8 Gyr, and metallicity as Z = 0.008. Moreover, Tadross (2005) analysed the cluster with regard to the radial profile of van den Bergh & Sher (1960) and estimated the core radius as  $r_c = 1'.4$ and the limiting radius as  $r_{\text{lim}} = 6'.5$ . Kyeong et al. (2008) applied a fitting procedure of the theoretical isochrones of Bertelli et al. (1994) to the colormagnitude diagrams based on CCD UBVI photometric data of NGC 1193. They calculated the color excess as  $E(B-V) = 0.19 \pm 0.04$  mag, the metallicity  $[Fe/H] = -0.45 \pm 0.12$  dex, the true distance module  $(m-M_{\rm V})_0=13.30\pm0.15$  mag, and the cluster age as  $\log t(yr) = 9.7 \pm 0.1$ .

The *Gaia* mission (Gaia collaboration et al. 2016) has led to substantial improvements in the quality and precision of astrometric, photometric,

and spectroscopic data. Gaia has provided precise astrometric, photometric, and spectroscopic data of nearly 1.8 billion stars. Cantat-Gaudin et al. (2018) identified 215 most likely cluster members, using astrometric and photometric data of stars across the locality of NGC 1193. In the study, they determined the mean proper motion of the cluster as  $(\mu_{\alpha}\cos\delta, \mu_{\delta}) = (-0.125 \pm 0.023, -0.329 \pm 0.000)$ 0.019) mas yr<sup>-1</sup> and the trigonometric parallax as  $\varpi = 0.159 \pm 0.009$  mas. Soubiran et al. (2018) used the second Gaia data release (Gaia DR2; Gaia collaboration et al. 2018) spectroscopy to identify a radial velocity measurement for one member star of NGC 1193, calculating its radial velocity as  $\langle V_{\rm r} \rangle =$  $-83.24 \pm 0.51$  km s<sup>-1</sup>. In addition, Carrera et al. (2019) determined the mean radial velocity of the cluster as  $\langle V_{\rm r} \rangle = -85.16 \; \rm km \; s^{-1}$ , based on APOGEE spectroscopic data for two member stars of the cluster. Donor et al. (2020) analysed three cluster member stars using APOGEE DR16 spectroscopic data and calculated the radial velocity and metallicity of the NGC 1193 as  $\langle V_{\rm r} \rangle = -84.7 \pm 0.2 \ {\rm km \ s^{-1}}$ and  $[Fe/H] = -0.34 \pm 0.01$  dex, respectively. Using Gaia DR2 data, they determined the mean proper motion components of the cluster as  $(\mu_{\alpha} \cos \delta)$ ,  $\mu_{\delta}$ )=(-0.22 ± 0.10, -0.36 ± 0.07) mas yr<sup>-1</sup>.

#### 1.2. NGC 1798

The open cluster NGC 1798 ( $\alpha=05^{\rm h}11^{\rm m}39^{\rm s}.36$ ,  $\delta=+47^{\circ}41^{'}27^{''}.60$ ,  $l=160^{\circ}.7043$ ,  $b=+04^{\circ}.8500$ ) was discovered in 1885 by Edward Barnard, located in the Auriga constellation (Dreyer 1888). With an angular size of about 5 arcmin, this cluster is classified as II2m with a central dense stellar concentration (Ruprecht 1966). Examination of the cluster's CMD reveals that the regions of the main sequence and red clump (RC) stars are more distinct than the red giant branch (RGB). Based on this morphological feature, Janes & Phelps (1994) gave the age of NGC 1798 as 1.5 Gyr and the distance as 3.44 kpc.

The first CCD UBVI photometric observations of the NGC 1798 were made by Park & Lee (1999). The angular diameter of the cluster was given as 8.3 arcmin (10.2 pc), the color excess  $E(B-V)=0.51\pm0.04$  magnitude, the distance  $d=4.2\pm0.3$  kpc, the metallicity [Fe/H] =  $-0.47\pm0.15$  dex, and the age  $t=1.4\pm0.2$  Gyr. Lata et al. (2002) used the data of Park & Lee (1999) to determine the absolute magnitude and color indices for the I band as  $I(M_{\rm V})=-4.86,\ I(U-V)_0=0.97,\ I(B-V)_0=0.82,\ {\rm and}\ I(V-I)_0=1.14$  mag. Maciejewski & Niedzielski (2007) obtained the structural and astrophysical parameters of 42 open clustical structural stru

ters with CCD BV photometry. They determined the cluster's limiting radius  $r_{\rm lim} = 9$  arcmin, the core radius  $r_{\rm c} = 1.3 \pm 0.1$  arcmin, the central stellar density  $f_0 = 9.5 \pm 0.28 \text{ star arcmin}^{-2}$ , and the background stellar density  $f_{\rm bg} = 3.14 \pm 0.05$  stars per arcmin<sup>2</sup>. These researchers used the isochrones of Bertelli et al. (1994), obtaining the color excess of the cluster as  $E(B-V) = 0.37^{+0.10}_{-0.09}$ , the distance modulus as  $(m-M) = 13.90^{+0.26}_{-0.63}$  mag, the distance as  $d = 3.55^{+0.64}_{-1.22}$  kpc, and the age being log t (w)  $\log t$  (yr) = 9.2. Ahumada & Lapasset (2007) examined 1,887 blue straggler star (BSS) candidates in 427 open clusters and identified 24 BSS in the direction of NGC 1798. They indicated that six of these BSS are massive and 18 are low mass stars. Carrera (2012) calculated the radial velocities of four open clusters including NGC 1798 by analyzing spectroscopic data of their member stars. By measuring Ca II lines, Carrera (2012) determined the mean radial velocity of NGC 1798 as  $\langle V_{\rm r} \rangle = 2 \pm 10 \ {\rm km \ s^{-1}}$ . They used six member stars in total, consisting of five RGB stars and one main sequence turn-off star. Oralhan et al. (2015) analyzed CCD UBVRI photometric observations of 20 open clusters and obtained their astrophysical parameters. They determined the reddening, photometric metallicity, distance modulus, distance, and age of the NGC 1798 as  $E(B-V) = 0.47 \pm 0.07$  mag, [Fe/H] =  $-0.50 \pm$  $0.28 \text{ dex}, (m-M)_0 = 12.70 \pm 0.04 \text{ mag}, d =$  $3.47 \pm 0.06$  kpc, and  $t = 1.78 \pm 0.22$  Gyr.

Cantat-Gaudin et al. (2020) used photometric and astrometric data from the Gaia DR2 (Gaia collaboration et al. 2018) to determine astrometric and astrophysical parameters of 2,017 open clusters. They identified 218 member stars in NGC 1798. Considering these members they calculated mean proper-motion components and trigonometric parallaxes of the cluster as  $(\mu_{\alpha}\cos\delta,\mu_{\delta})=(0.913\pm0.011,-0.318\pm0.010)$  mas yr<sup>-1</sup> and  $\varpi=0.178\pm0.005$  mas. Liu & Pang (2019) used astrometric and photometric data of 78 member stars of NGC 1798 to calculate the mean proper-motion components, trigonometric parallaxes, and age of the cluster as  $(\mu_{\alpha}\cos\delta,\mu_{\delta})=(0.903\pm0.026,-0.400\pm0.295)$  mas yr<sup>-1</sup>,  $\varpi=0.241\pm0.026$  mas, and  $t=1.7\pm0.1$  Gyr.

A number of studies explored open clusters using ground-based telescopes within the scope of spectroscopic survey programs (Gilmore et al. 2012; Conrad et al. 2014; Maciejewski & Niedzielski 2007; Kos et al. 2018). Within the context of the APOGEE survey, Donor et al. (2018) utilized spectral observations of 259 cluster member stars in 19 open clusters including NGC 1798 and obtained the radial ve-

locity and different metal abundance values of the stars. Analysing nine member stars in NGC 1798 Donor et al. (2018) determined the mean radial velocity as  $\langle V_r \rangle = 2 \pm 1.7 \text{ km s}^{-1}$  and the iron abundance  $[Fe/H] = -0.18 \pm 0.02$  dex. Soubiran et al. (2018) analysed Gaia DR2 spectroscopic data of four member stars in the cluster and obtained the mean radial velocity as  $\langle V_{\rm r} \rangle = 2.60 \pm 0.41 \; \rm km \; s^{-1}$ . Donor et al. (2020) analysed eight cluster member stars using APOGEE DR16 spectroscopic data and calculated the radial velocity and metallicity of the NGC 1798 as  $\langle V_{\rm r} \rangle = 2.7 \pm 0.8 \; \rm km \; s^{-1}$  and  $[Fe/H] = -0.27 \pm 0.03$  dex, respectively. Using Gaia DR2 data, they determined the mean proper motion components of the cluster as  $(\mu_{\alpha}\cos\delta, \mu_{\delta})=(0.83\pm$  $0.04, -0.31 \pm 0.04)$  mas yr<sup>-1</sup>.

#### 2. OBSERVATIONS AND DATA REDUCTIONS

#### 2.1. CCD UBV Photometric Data

The observations of these two clusters, along with many others, were carried out at the San Pedro Martir Observatory,  $^6$  as part of an ongoing UBVRI photometric survey of Galactic stellar clusters. The 84-cm (f/15) Ritchey-Chretien telescope was employed in combination with the Mexman filter wheel.

NGC 1193 was observed on 2013-09-19 with the ESOPO CCD detector (a 2048  $\times$  2048 13.5- $\mu$ m square-pixels E2V CCD42-40 with a gain of 1.65 e<sup>-</sup>/ADU and a readout noise of 3.8 e<sup>-</sup> at the 2  $\times$  2 binning employed, providing an unvignetted field of view of 7.4  $\times$  9.3 arcmin<sup>2</sup>). Short and long exposures were taken to properly measure both the bright and faint stars of the fields. Exposure times were 2, 12, 120s for both I and R; 6, 30, 200 for V; 30, 100, 700s for B; and 60 and 1800s for U.

NGC 1798 was observed on 2009-11-01 with the SITE3 detector (a Photometrics  $1024 \times 1024$  24- $\mu$ m square-pixels with a gain of  $1.3\,\mathrm{e^-/ADU}$  and a readout noise of  $6.8\,\mathrm{e^-}$ , giving an unvignetted field of view of  $6.8 \times 6.8$  arcmin<sup>2</sup>). Exposure times for I and R were 2, 12 and 120s in duration; 6, 30 and 200s for V; 30, 100 and 700s for B; and 60 and 1800s for U.

Landolt's standard stars (Landolt 2009) were also observed in good sky conditions, at the meridian and at about two air masses, to properly determine the atmospheric extinction coefficients. Flat fields were taken at the beginning and the end of each night and bias images were obtained between cluster observations. Data reduction with point spread function (PSF) photometry was carried out by one of

 $<sup>^6 {\</sup>rm https://www.astrossp.unam.mx/en/home/.}$ 

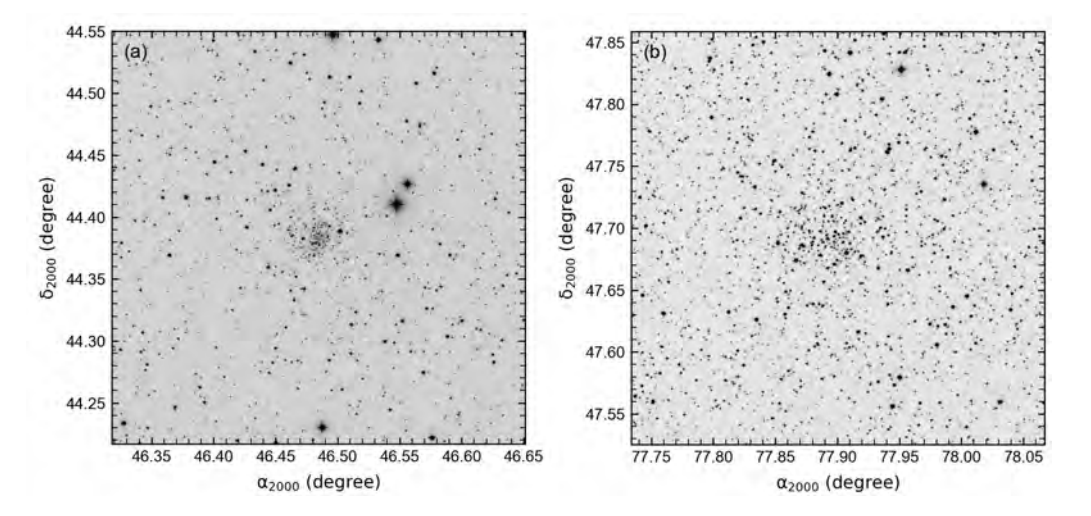


Fig. 1. Identification charts for NGC 1193 (left panel) and NGC 1798 (right panel), taken from the Leicester database and archive service (LEDAS).

the authors (RM) with the IRAF/DAOPHOT packages (Stetson 1987) and employing the transformation equations recommended, in their Appendix B, by Stetson et al. (2019).

#### 3. DATA ANALYSIS

#### 3.1. Gaia Astrometric and Photometric Data

The (early) third data release of Gaia (hereafter Gaia EDR3, Gaia collaboration et al. 2021) provides high quality astrometric and photometric data of nearly 1.5 billion celestial objects. gether with ground-based CCD UBV photometry we took into account Gaia EDR3 astrometric and photometric data to perform astrometric, photometric, and kinematic analyses of NGC 1193 and NGC 1798. We extracted such EDR3 data for all stars within regions of 20 arcmins about the centres of each cluster, using the coordinates given by Cantat-Gaudin et al. (2020) ( $\alpha = 03^{\rm h}05^{\rm m}56.64$ ,  $\delta =$  $+44^{\circ}22'58''.80$  for NGC 1193 and  $\alpha = 05^{\rm h}11^{\rm m}39^{\rm s}.36$ ,  $\delta = +47^{\circ}41'27''.60$  for NGC 1798). Thus we reached 9,141 stars within the magnitude range 7 < G <23 mag for NGC 1193 and 14.834 stars within 8 <G < 21 mag for NGC 1798, respectively. 20 arcmin field of view optical images for the two clusters are presented in Figure 1. To construct photometric and astrometric catalogues for each cluster, we matched the UBV data to that from the Gaia EDR3 catalogue using stellar equatorial coordinates considering distances less than 5 arcsec. The mean difference in distances between the coordinates of stars in the matched catalogues was  $\approx 0.08$  arc seconds for both clusters. Both resulting catalogues contain positions  $(\alpha, \delta)$ , UBV observational data (apparent V magnitudes, color indices U - B, B - V), Gaia EDR3 astrometric  $(\mu_{\alpha}\cos\delta,\mu_{\delta},\ \varpi)$  and photometric data  $(G, G_{BP} - G_{RP})$ , and membership probabilities (P)as calculated in this study (Table 1). Catalogues of CCD UBV photometric as well as Gaia photometric and astrometric data for all the detected stars in the cluster regions are available electronically for NGC 1193 and NGC 1798 $^7$ . Errors of the UBV and Gaia EDR3 photometric data were adopted as internal errors, being the uncertainties in the determination of the instrumental magnitudes of the stars. We calculated the mean photometric errors separately as functions of V and G intervals, listing the results in Table 2 (on page 338). It can be seen from the table that the mean internal UBV errors reach 0.08 mag for stars brighter than V = 20 mag for both clusters. The mean internal errors of Gaia EDR3 photometry for stars brighter than G = 21 mag reach 0.011 mag for NGC 1193 and 0.007 mag for NGC 1798.

To obtain precise astrophysical parameters, we identified photometric completeness limits for each cluster. Stars fainter that these limits were not included in further analyses. G and V magnitude histograms were constructed to determine the photometric completeness limits for each clusters (see Figure 2). Stellar counts decrease for magnitudes fainter than G=20 for both NGC 1193 (Figure 2a) and NGC 1798 (Figure 2c). Stellar counts decrease for magnitudes fainter than V=19 for NGC 1193 (Figure 2b) and NGC 1798 (Figure 2d), indicating that incompleteness (of stellar recovery) has set in. Thus, for both clusters, we adopted these values as the cluster photometric completeness limits.

 $<sup>^7{\</sup>rm The}$  complete tables can be obtained from VizieR electronically.

TABLE 1: THE PHOTOMETRIC AND ASTROMETRIC CATALOGUES FOR NGC 1193 and NGC 1798

	Ь			0.80	0.00	0.00	1.00	:	0.00	0.30	0.00	0.00	0.40		Ь		0.32	0.29	0.00	0.00	0.35	:	08.0	0.00	0.98	0.00	0.00
	β	(mas)		-0.083(0.241)	1.009(0.177)	0.640(0.214)	0.185(0.220)	÷	0.433(0.119)	0.149(0.121)	0.604(0.036)	0.799(0.068)	0.264(0.521)		В	(mas)	0.270(0.344)	-0.051(0.289)	0.083(0.140)	0.418(0.279)	0.144(0.143)	:	0.119(0.059)	0.354(0.074)	0.289(0.043)	0.947(0.336)	0.906(0.305)
	$\mu_{\delta}$	$(\text{mas yr}^{-1})$	1	-0.251(0.223)	-0.566(0.165)	-2.553(0.200)	-0.410(0.235)	:	-2.394(0.097)	-0.447(0.122)	-2.523(0.030)	-1.965(0.062)	0.166(0.412)		$\mu_{\delta}$	$(\text{mas yr}^{-1})$	-0.986(0.343)	-0.611(0.283)	-0.596(0.137)	-2.917(0.270)	-1.461(0.141)	:	-1.241(0.059)	-3.354(0.077)	-0.518(0.043)	-1.480(0.356)	0.057(0.294)
	$\mu_{\alpha}\cos\delta$	$(\text{mas yr}^{-1})$		-0.587(0.247)	-4.640(0.181)	-4.072(0.220)	-0.426(0.220)	÷	1.640(0.128)	-0.717(0.177)	-5.602(0.039)	5.074(0.078)	0.254(0.530)		$\mu_{\alpha}\cos\delta$	$(\text{mas yr}^{-1})$	0.968(0.426)	0.919(0.372)	-0.020(0.175)	1.623(0.331)	0.913(0.171)	:	0.843(0.073)	0.805(0.098)	0.701(0.056)	-1.779(0.431)	0.414(0.358)
	$G_{ m BP}-G_{ m RP}$	(mag)	1.693(0.116)	1.080(0.043)	2.116(0.035)	1.759(0.040)	0.969(0.032)	:	1.137(0.014)	0.786(0.020)	0.908(0.005)	1.235(0.008)	1.061(0.069)		$G_{\mathrm{BP}}-G_{\mathrm{RP}}$	(mag)	1.573(0.056)	1.575(0.048)	1.471(0.024)	1.604(0.057)	1.315(0.025)	:	1.623(0.008)	1.322(0.008)	0.870(0.005)	1.875(0.036)	1.461(0.057)
3	Ċ	(mag)	21.929(0.049)	18.777(0.003)	18.254(0.003)	18.592(0.003)	18.418(0.003)	:	17.510(0.003)	17.463(0.003)	15.287(0.003)	16.465(0.003)	19.655(0.005)	80	Ŋ	(mag)	19.499(0.004)	19.278(0.004)	18.215(0.003)	19.369(0.004)	18.291(0.003)	:	16.766(0.003)	17.158(0.003)	15.582(0.003)	19.037(0.004)	19.339(0.004)
NGC 1193	B-V	(mag)	1.155(0.120)	0.893(0.083)	1.475(0.140)	1.262(0.137)	0.993(0.065)	:	0.881(0.026)	0.616(0.020)	0.697(0.008)	0.941(0.044)	0.658(0.152)	NGC 1798	B-V	(mag)	0.563(0.192)	1.182(0.171)	1.046(0.074)	0.920(0.208)	1.050(0.071)	:	1.321(0.046)	0.913(0.040)	0.551(0.043)	1.848(0.043)	0.931(0.298)
	U - B	(mag)					0.194(0.170)	:	0.458(0.088)	0.042(0.042)	0.058(0.011)	0.534(0.156)			U - B	(mag)	1				-0.360(0.265)	:	0.807(0.267)	0.286(0.162)	0.281(0.038)		
	Λ	(mag)	19.194(0.062)	18.984(0.044)	19.162(0.056)	19.286(0.067)	18.631(0.034)	÷	17.758(0.017)	17.558(0.014)	15.451(0.006)	16.806(0.042)	19.881(0.101)		Λ	(mag)	20.254(0.135)	19.765(0.089)	18.623(0.041)	20.046(0.151)	18.459(0.045)	:	17.366(0.020)	17.628(0.024)	15.629(0.040)	19.197(0.028)	20.344(0.191)
	DEC	(dd:mm:ss.ss)	+44:22:00.62	+44:22:01.67	+44:19:33.12	+44:21:46.02	+44:24:25.10	:	+44:18:51.83	+44:24:53.68	+44:19:29.22	+44:27:38.77	+44:18:25.54		DEC	(dd:mm:ss.ss)	+47:39:52.01	+47:38:35.08	+47:41:26.68	+47:43:15.08	+47:44:05.70	:	+47:38:31.88	+47:38:58.99	+47:38:05.24	+47:39:49.94	+47:42:42.85
	$_{ m RA}$	(hh:mm:ss.ss)	03.05.36.67	03:05:37.44	03:05:38.33	03:05:38.40	03:05:38.74	:	03:06:18.54	03:06:19.07	03:06:19.29	03:06:19.45	03:06:19.77		RA	(hh:mm:ss.ss)	05:11:19.70	05:11:19.73	05:11:19.79	05:11:20.00	05:11:20.13	:	05:11:58.51	05:11:58.73	05:11:58.88	05:11:59.04	05:11:59.15
	П		001	005	003	004	002	i	292	266	267	268	269		П		001	005	003	004	002	:	523	524	525	526	527

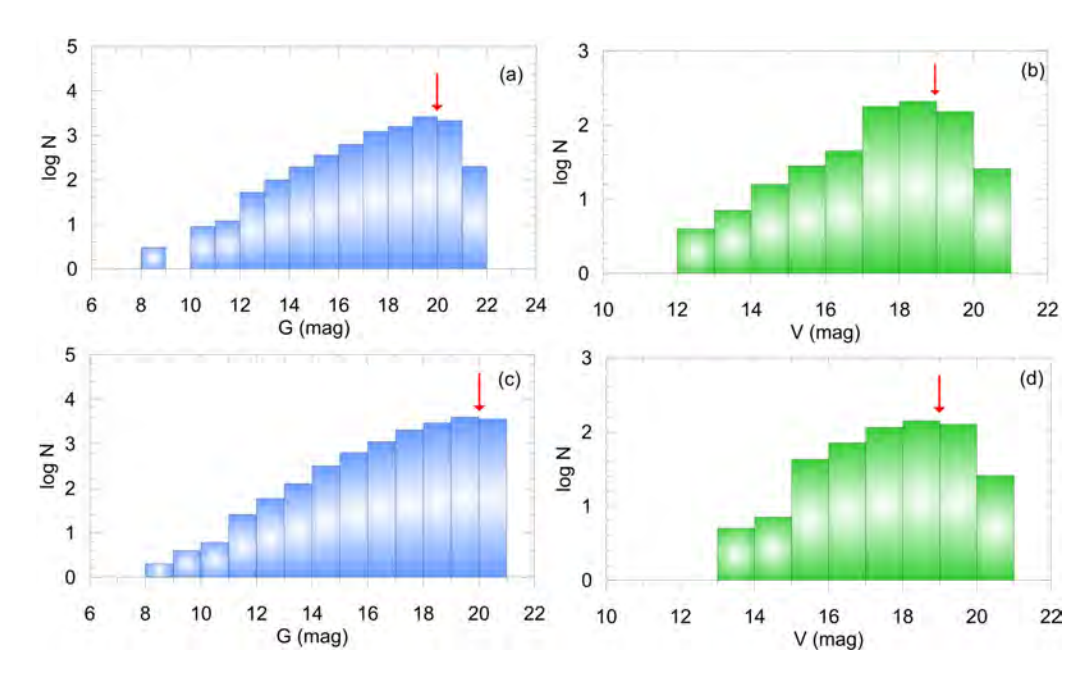


Fig. 2. Interval G and V-band magnitude histograms of NGC 1193 (a, b) and NGC 1798 (c, d): The red arrows show the faint limiting apparent magnitudes in G and V-bands. The color figure can be viewed online.

 ${\it TABLE~2}$  THE MEAN INTERNAL PHOTOMETRIC ERRORS FOR EACH CLUSTER

		NGC 119	03			N	GC 1798	
V	N	$\sigma_{ m V}$	$\sigma_{ m U-B}$	$\sigma_{ m B-V}$	N	$\sigma_{ m V}$	$\sigma_{ m U-B}$	$\sigma_{ m B-V}$
(8, 12]	_	_	_	_		_	_	_
(12, 14]	9	0.017	0.020	0.022	5	0.024	0.047	0.045
(14, 15]	14	0.008	0.012	0.010	5	0.027	0.054	0.038
(15, 16]	22	0.007	0.018	0.010	41	0.021	0.055	0.032
(16, 17]	36	0.011	0.037	0.015	70	0.020	0.070	0.033
(17, 18]	147	0.018	0.065	0.027	114	0.023	0.148	0.037
(18, 19]	177	0.034	0.122	0.057	140	0.045	0.230	0.075
(19, 20]	140	0.075	0.234	0.130	126	0.077	_	0.141
(20, 21]	24	0.145	_	0.244	26	0.136	_	0.242
		NGC 119	)3			N	GC 1798	
G	N	$\sigma_{ m G}$	$\sigma_{G_{\mathrm{BP}}-G_{\mathrm{RP}}}$		N	$\sigma_{ m G}$	$\sigma_{G_{\mathrm{BP}}-G_{\mathrm{RP}}}$	
(5, 10]	5	0.003	0.006		6	0.003	0.005	
(10, 12]	21	0.003	0.005		32	0.003	0.005	
(12, 13)	52	0.003	0.005		59	0.003	0.005	
(13, 14]	101	0.003	0.005		125	0.003	0.005	
(14, 15]	196	0.003	0.006		315	0.003	0.005	
(15, 16]	366	0.003	0.006		630	0.003	0.006	
(16, 17]	634	0.003	0.010		1115	0.003	0.009	
(17, 18]	1219	0.003	0.019		2026	0.003	0.017	
(18, 19]	1588	0.004	0.044		2936	0.003	0.035	
(19, 20]	2616	0.005	0.155		3943	0.004	0.075	
(20, 21]	2144	0.011	0.232		3647	0.007	0.152	
(21, 23]	198	0.027	0.378					

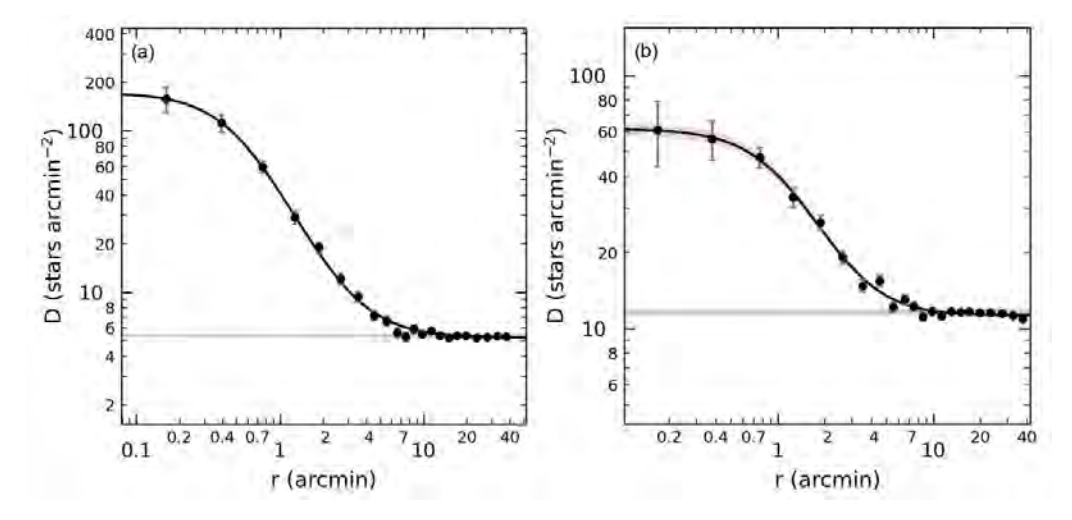


Fig. 3. Radial density profiles for NGC 1193 (a) and NGC 1798 (b). Errors were derived using the equation of  $1/\sqrt{N}$ , where N represents the number of stars used in the density estimation. The solid lines represents the optimal King (1962) profiles. The background density level and its errors are the horizontal grey bands. The King fit uncertainty  $(1\sigma)$  is shown by the red shaded region. The color figure can be viewed online.

#### 3.2. Structural Parameters of the Clusters

We utilized Radial Density Profile (RDP) analvsis to determine the structural parameters of the clusters. First, we specified many concentric rings outwards from the cluster center, using the central coordinates given by Cantat-Gaudin et al. (2020). Stellar densities  $(\rho)$  were estimated for each ring by dividing the number of stars within the photometric completeness limit (G < 20 mag) in it by the ring area. The resulting RDPs were fitted with King (1962) models via  $\chi^2$  minimisation, giving estimates for the core, limiting, and effective radii of each cluster. The King (1962) model is described as  $\rho(r) =$  $f_{\rm bg} + [f_0/(1 + (r/r_{\rm c})^2)]$  where r is the radius from the cluster centre,  $f_{\rm bg}$  the background density,  $f_0$ the central density, and  $r_{\rm c}$  the core radius. See Figure 3 for each cluster's RDP together with the best fitting King (1962) model to it. As a result of the fitting procedure, we inferred central stellar density, core radius and background stellar density as  $f_0 =$  $166.865\pm1.573 \,\mathrm{stars \, arcmin^{-2}}, \, r_{\rm c} = 0.526\pm0.009 \,\mathrm{ar}$ cmin and  $f_{\rm bg} = 5.225 \pm 0.124 {\rm stars arcmin}^{-2} {\rm for}$ NGC 1193 and  $f_0 = 53.597 \pm 3.789 \text{ stars arcmin}^{-2}$ ,  $r_{\rm c} = 1.190 \pm 0.056$  arcmin and  $f_{\rm bg} = 11.318 \pm$ 0.321 stars arcmin<sup>-2</sup> for NGC 1798, respectively. At the r=8 arcmin limiting radius, the stellar density becomes similar to the background density (a grey horizontal line) as seen in Figure 3a (NGC 1193) and Figure 3b (NGC 1798). Therefore, we concluded that the limiting radii for both clusters are  $r_{\rm lim} = 8$  arcmin. We considered only the stars inside these limiting radii in further analyses.

#### 3.3. CMDs and Membership Probabilities of Stars

The membership probabilities (P) of stars located in each of two cluster regions were calculated applying the Unsupervised Photometric Membership Assignment in Stellar Cluster program (UP-MASK; Krone-Martins & Moitinho 2014). UPMASK uses k-means clustering, where k is the number of clusters, to detect spatially concentrated groups and identify the most likely cluster members. An integer k-means is not adjusted directly by the user and the best result from the UPMASK methodology is achieved when the k-means value is within 6 to 25 (Krone-Martins & Moitinho 2014; Cantat-Gaudin et al. 2020). We applied UPMASK to calculate stellar membership probabilities by considering each star's five-dimensional astrometric parameters from Gaia EDR3 (Gaia collaboration et al. 2021), which contains equatorial coordinates  $(\alpha, \delta)$ , proper motion components  $(\mu_{\alpha}\cos\delta, \mu_{\delta})$ , trigonometric parallaxes  $(\varpi)$ , and their uncertainties. During application we scaled these five parameters to unit variance and ran 100 iterations for each clusters to assess cluster membership. The membership probability of a star is defined by the frequency of the group in which it is clustered. We reached the best results when k was set to 12 for NGC 1193 and 15 for NGC 1798. We identified as possible cluster members those stars brighter than G=20 mag with membership probabilities P>0.5that we identified as possible members of clusters. This led to 735 possible members for NGC 1193 and 1,536 for NGC 1798. Cantat-Gaudin et al. (2020) give the number of stars brighter than G = 18 mag

with the membership probabilities P > 0.5 as 215 for NGC 1193 and 218 for NGC 1798. The dissimilarity can be explained by lower precision in the astrometric Gaia DR2 data compared to Gaia EDR3, as well as the G magnitude limit of stars used in the analyses. With the release of Gaia EDR3 data, the precision of astrometric and photometric measurements increased with respect to Gaia EDR2 data. For the Gaia EDR3 release the accuracy of trigonometric parallaxes increased by 30 percent and the uncertainties decreased by nearly 40%, the proper motion accuracy increased by a factor of 2 and the associated uncertainties improved by a factor  $\approx 2.5$ . Moreover, the precision of photometric data and celestial positions are better in terms of homogeneity (Gaia collaboration et al. 2021).

To take into consideration the impact of binary stars in the main-sequences of the studied clusters. we plotted the  $V \times (B - V)$  CMDs of the stars within the cluster limiting radii  $(r_{lim})$  which we had obtained for the clusters and then fitted the Zero Age Main-Sequence (ZAMS) of Sung et al. (2013) to these diagrams. The ZAMS fitting was by eye according to the stars with the membership probability  $P \geq 0.5$  and shifted 0.75 mag towards brighter magnitudes in order to account for the most likely cluster binary stars (4a and c). During the ZAMS fitting we made sure for each cluster that the mainsequence, turn-off, and giant stars with membership probabilities P > 0.5 were selected. The process resulted in 181 likely member stars for NGC 1193 and 161 for NGC 1798 which lie between the fitted ZAMS curves and are located inside the  $r_{\rm lim}$ radii. We used these stars to determine astrophysical parameters of the two clusters. Figure 4 shows the  $V \times (B - V)$  CMDs with the best fitted ZAMS (Figures 4a and c) and  $G \times (G_{BP} - G_{RP})$  CMDs (Figures 4b and d) with the background and most likely member stars. Figure 5 presents histograms of the number of stars located through the two cluster fields versus their membership probabilities. Vector-Point Diagrams (VPDs) were plotted for the stars within the limiting radii and are shown as Figure 6. It can be seen from the figure that NGC 1193 (Figure 6a) and NGC 1798 (Figure 6b) are affected by field stars but with the membership selection criteria, the 'most likely' cluster stars (shown as the colorscaled points in Figure 6) can be separated from field stars (grey dots in Figure 6). The mean proper motion components of the most likely cluster members are  $(\mu_{\alpha}\cos\delta, \mu_{\delta}) = (-0.207 \pm 0.009, -0.431 \pm$ 0.008) for NGC 1193 and  $(\mu_{\alpha}\cos\delta, \mu_{\delta}) = (0.793 \pm$  $0.006, -0.373 \pm 0.005$ ) mas yr<sup>-1</sup> for NGC 1798.

Moreover, using these members we obtained mean trigonometric parallaxes of NGC 1193 and NGC 1798 as  $\varpi_{Gaia} = 0.191 \pm 0.157$  mas and  $\varpi_{Gaia} = 0.203 \pm 0.099$  mas, respectively.

## 4. ASTROPHYSICAL PARAMETERS OF THE CLUSTERS

We summarize in this section the processes we performed to determine the astrophysical parameters of NGC 1193 and NGC 1798 (for detailed descriptions on the methodology see Yontan et al. 2015, 2019, 2021; Ak et al. 2016; Bilir et al. 2006, 2010, 2016; Bostancı et al. 2015, 2018; Banks et al. 2020; Akbulut et al. 2021; Koç et al. 2022). Color excesses and metallicities of the clusters were derived using two-color diagrams (TCDs), whereas we obtained distance moduli and ages individually by fitting theoretical models on CMDs.

#### 4.1. Reddening

The E(U-B) and E(B-V) color excesses for NGC 1193 and NGC 1798 were derived using  $(U-B)\times (B-V)$  TCDs. We selected the mainsequence stars for which simultaneous U, B, and Vmagnitudes were available, as well as with membership probabilities  $P \geq 0.5$ . As shown in Figure 7, we constructed TCDs for these stars and compared their positions by fitting the solar metallicity dereddened ZAMS of Sung et al. (2013). The ZAMS was fitted according to the equation E(U-B) = $0.72 \times E(B-V) + 0.05 \times E(B-V)^2$  (Garcia et al. 1988) by applying  $\chi^2$  optimisation with steps of 0.001 mag. The best solutions for E(B-V) and E(U-B) values are those corresponding to the minimum  $\chi^2$ , being  $E(B-V) = 0.150 \pm 0.037$  mag for NGC 1193 and  $E(B-V) = 0.505 \pm 0.100$  mag for NGC 1798. The errors of color excesses are determined as  $\pm 1\sigma$  deviations, and are presented as the green lines in Figure 7. When we compared the reddening estimated for NGC 1193, we concluded that it is in a good agreement within the errors with the values  $(0.10 \le E(B-V) \le 0.19 \text{ mag})$  given by different authors (Kaluzny 1988; Tadross 2005; Kyeong et al. 2008). For NGC 1798, our finding result is compatible with the values given by Park & Lee (1999,  $E(B-V) = 0.51 \pm 0.04$  mag) and Oralhan et al.  $(2015, E(B-V) = 0.47 \pm 0.07 \text{ mag}).$ 

#### 4.2. Metallicities

The determination of photometric metallicities of the two clusters employed the method given by Karaali et al. (2003a,b, 2011). This

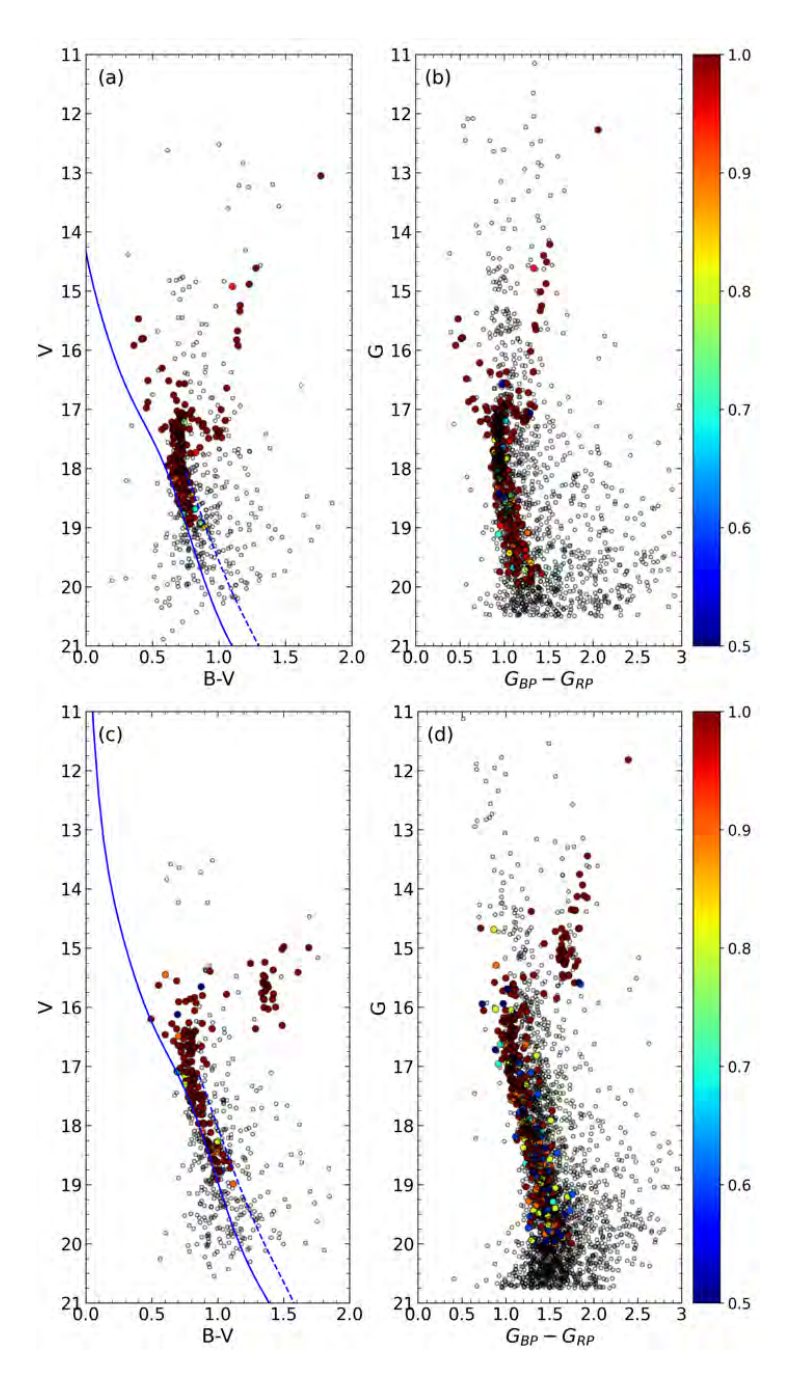


Fig. 4.  $V \times (B-V)$  and  $G \times (G_{\rm BP}-G_{\rm RP})$  CMDs of NGC 1193 (a, b) and NGC 1798 (c, d). The blue dot-dashed lines represent the ZAMS (Sung et al. 2013) including the binary star effect. The membership probabilities of stars that lie within the fitted ZAMS are shown with different colors according to the color scales shown to the right of the figure. These member stars are located within  $r_{\rm lim}=8$  arcmin of the cluster centres calculated for NGC 1193 and NGC 1798. Grey dots indicate low probability members (P < 0.5), or field stars (P = 0). The color figure can be viewed online.

method is based on F and G type mainsequence stars and their UV-excesses as well as on stars whose color index range correspond to  $0.3 \le (B-V)_0 \le 0.6$  mag (Eker et al. 2018, 2020). We selected F-G type main-sequence stars within the range  $0.3 \leq (B-V)_0 \leq 0.6$  mag after calculating the intrinsic  $(B-V)_0$  and  $(U-B)_0$  colors of the most likely cluster member  $(P \geq 0.5)$  stars. To determine the difference between the  $(U-B)_0$  color indices of cluster stars and the Hyades main sequence

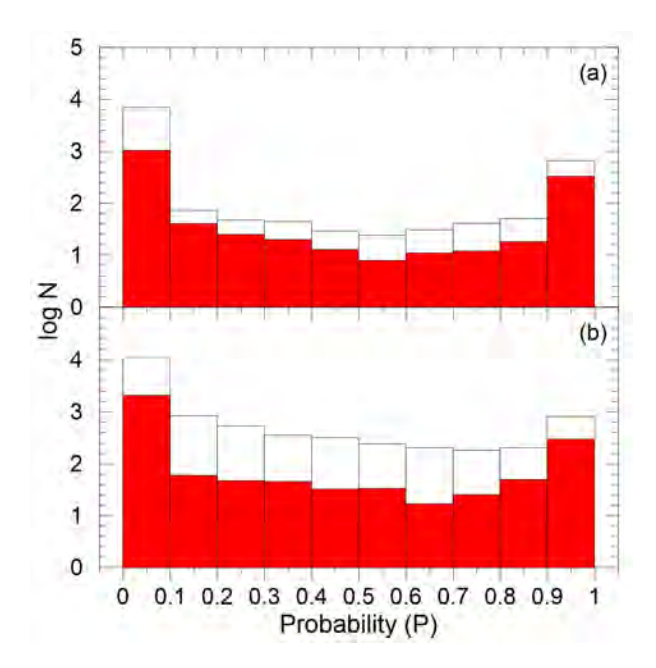


Fig. 5. Histograms of the membership probabilities for NGC 1193 (a) and NGC 1798 (b). The red colored shading denotes the stars that lie within the main-sequence band and effective cluster radii ( $r_{\rm lim} \leq 8'$ ), while the white colored bars indicate the membership probabilities of all stars in each cluster's direction. The color figure can be viewed online.

which corresponds to the same  $(B-V)_0$  color indices, we constructed  $(U-B)_0 \times (B-V)_0$  TCDs. This difference between cluster and Hyades stars is defined as the UV-excess which is expressed by the equation of  $\delta = (U-B)_{0,\mathrm{H}} - (U-B)_{0,\mathrm{S}}$ , where H and S denote the Hyades and cluster stars respectively, which implies the same  $(B-V)_0$  color indices. By calibrating  $(B-V)_0$  of stars to  $(B-V)_0 = 0.6$  mag (i.e.,  $\delta_{0.6}$ ) we normalised the UV excess and plotted the histogram of normalised  $\delta_{0.6}$  values. To calculate the mean  $\delta_{0.6}$ , we fitted a Gaussian to the distribution. Taking into account the Gaussian peak, the photometric metallicities of the studied clusters are obtained from the equation given by Karaali et al. (2011):

$$[Fe/H] = -14.316(1.919)\delta_{0.6}^2 - 3.557(0.285)\delta_{0.6} +0.105(0.039).$$
(1)

We identified 12 and 7 F-G type main-sequence stars to calculate the photometric metallicity of NGC 1193 and NGC 1798, respectively. TCDs and the distributions of normalised  $\delta_{0.6}$  UV excesses for two clusters are shown in Figure 8. The calculated mean  $\delta_{0.6}$  values of NGC 1193 and NGC 1798 are  $0.085\pm0.010$  mag and  $0.068\pm0.011$  mag, respec-

tively. The photometric metallicity [Fe/H] value for NGC 1193 is [Fe/H] =  $-0.30 \pm 0.06$  dex and for NGC 1798 it is [Fe/H] =  $-0.20 \pm 0.07$  dex, which correspond to their peak values in the  $\delta_{0.6}$  distribution.

The [Fe/H] metallicities were transformed to the mass fraction Z to derive ages of the clusters. For this, the analytic equations of Bovy<sup>8,9</sup> for PARSEC (Bressan et al. 2012) models were used, namely:

$$z_{\rm x} = 10^{[{\rm Fe/H}] + \log\left(\frac{z_{\odot}}{1 - 0.248 - 2.78 \times z_{\odot}}\right)},$$
 (2)

and

$$z = \frac{(z_{\rm x} - 0.2485 \times z_{\rm x})}{(2.78 \times z_{\rm x} + 1)}.$$
 (3)

z and  $z_{\rm x}$  are the elements heavier than helium and the intermediate operation function, respectively.  $z_{\odot}$  is the solar metallicity which was adopted as 0.0152 (Bressan et al. 2012). We calculated z=0.008 for NGC 1193 and z=0.010 for NGC 1798.

Many authors obtained spectroscopic metallicities of NGC 1193 and NGC 1798 based on ground-based observations, as listed in Table 3. Photometric metallicities calculated in this study are well supported by the spectroscopic studies presented in the literature. We conclude that our metallicity findings are reliable. Thus, we adopted our results for the determination of distance moduli and age.

#### 4.3. Distance Moduli and Age Estimation

We used Parsec isochrones (Bressan et al. 2012), which contain UBV filters as well as Gaia passbands, to obtain the distance moduli and ages of the studied clusters simultaneously. To do this, we selected the PARSEC models considering the mass fractions (z) estimated for each cluster and compared them to the  $V \times (U-B)$ ,  $V \times (B-V)$ , and  $G \times (G_{BP}-V)$  $G_{\rm RP}$ ) CMDs according to member stars  $(P \ge 0.5)$ . Selected isochrones were fitted to CMDs visually by attaching importance to 'most likely' member stars which make up the main-sequence, turn-off and giant regions of each cluster. During the fitting process of PARSEC models to the UBV data, we used the E(B-V) values derived above by this study, while for the Gaia EDR3 data we considered the equation of  $E(G_{BP} - G_{RP}) = 1.41 \times E(B - V)$  (Sun et al. 2021). We obtained the error of the distance moduli and distances using the relation given by Carraro et al. (2017). We fitted two more isochrones

<sup>8</sup>https://github.com/jobovy/isodist/blob/master/ isodist/Isochrone.py.

 $<sup>^9{\</sup>rm The}$  equations are given in lines between 199 and 207 in the code.

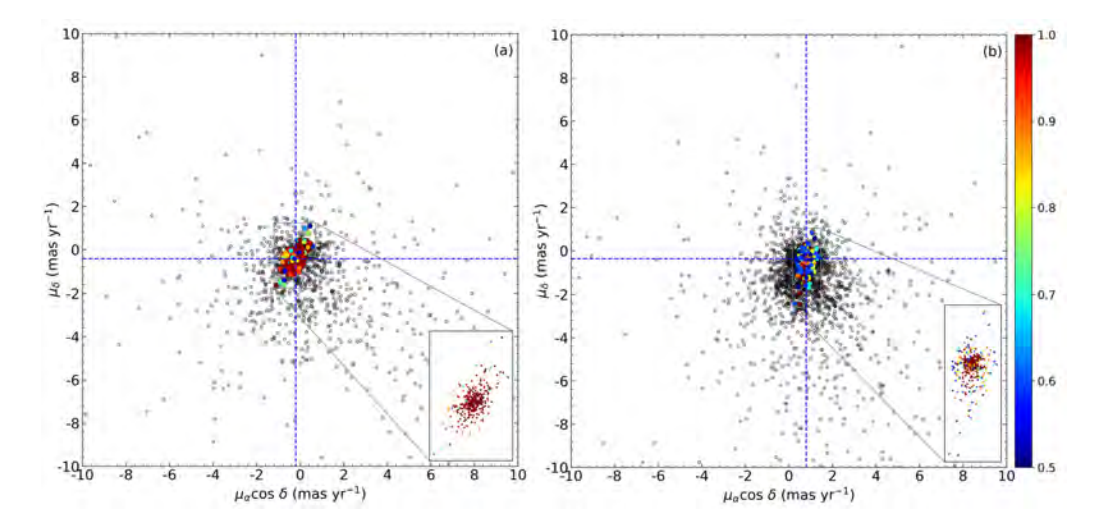


Fig. 6. VPDs of NGC 1193 (a) and NGC 1798 (b). Colored dots identify the membership probabilities of the most likely cluster members according to the color scale shown on the right. The zoomed box in the panels represents the region of condensation for both clusters in the VPD. Dashed lines are the intersection of the mean proper motion values. The color figure can be viewed online.

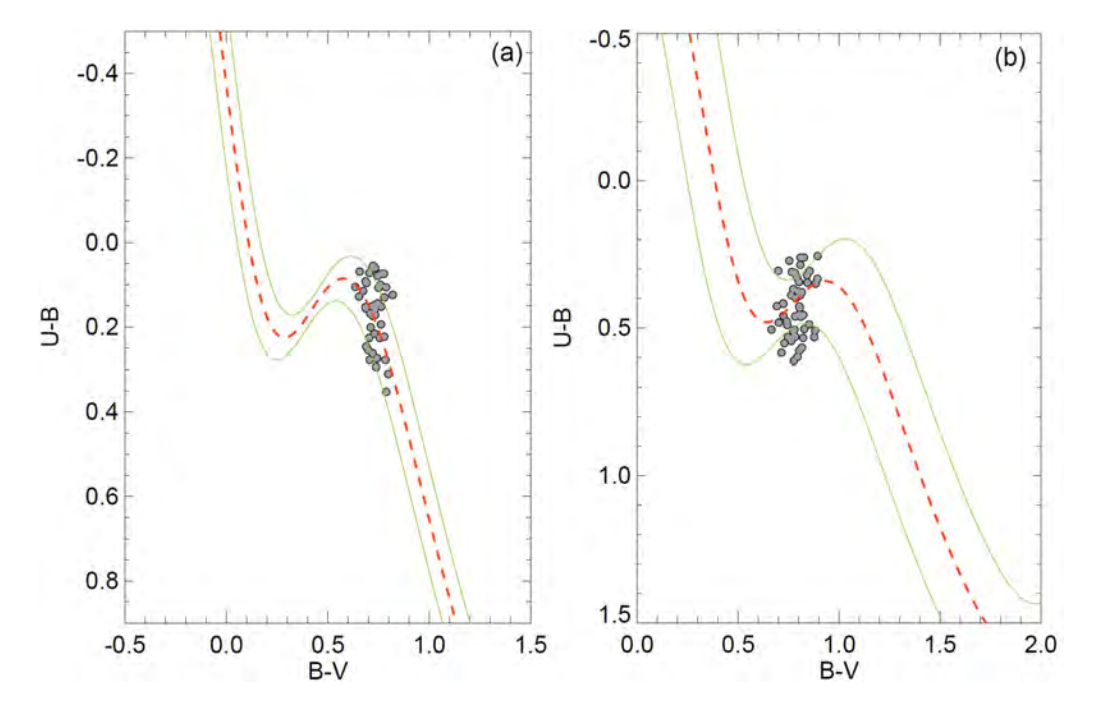


Fig. 7. Two-color diagrams of the most probable member main-sequence stars in the regions of NGC 1193 (a) and NGC 1798 (b). Red dashed and green solid curves represent the reddened ZAMS given by Sung et al. (2013) and  $\pm 1\sigma$  standard deviations, respectively. The color figure can be viewed online.

to estimate age uncertainties considering the spread of the most likely member stars in the turn-off and sub-giant regions of the cluster. The ages of such selected isochrones give the higher and lower acceptable values for the estimated cluster ages. The best fit with z=0.008 gave the distance moduli and age

of NGC 1193 as  $\mu=14.191\pm0.149$  mag and  $t=4.6\pm1.0$  Gyr. For NGC 1798, the best fit of z=0.010 gave these values as  $\mu=14.808\pm0.332$  mag and  $t=1.3\pm0.2$  Gyr, respectively. The distances of the clusters corresponding to the estimated distance moduli are also  $d_{\rm iso}=5562\pm381$  pc for NGC 1193

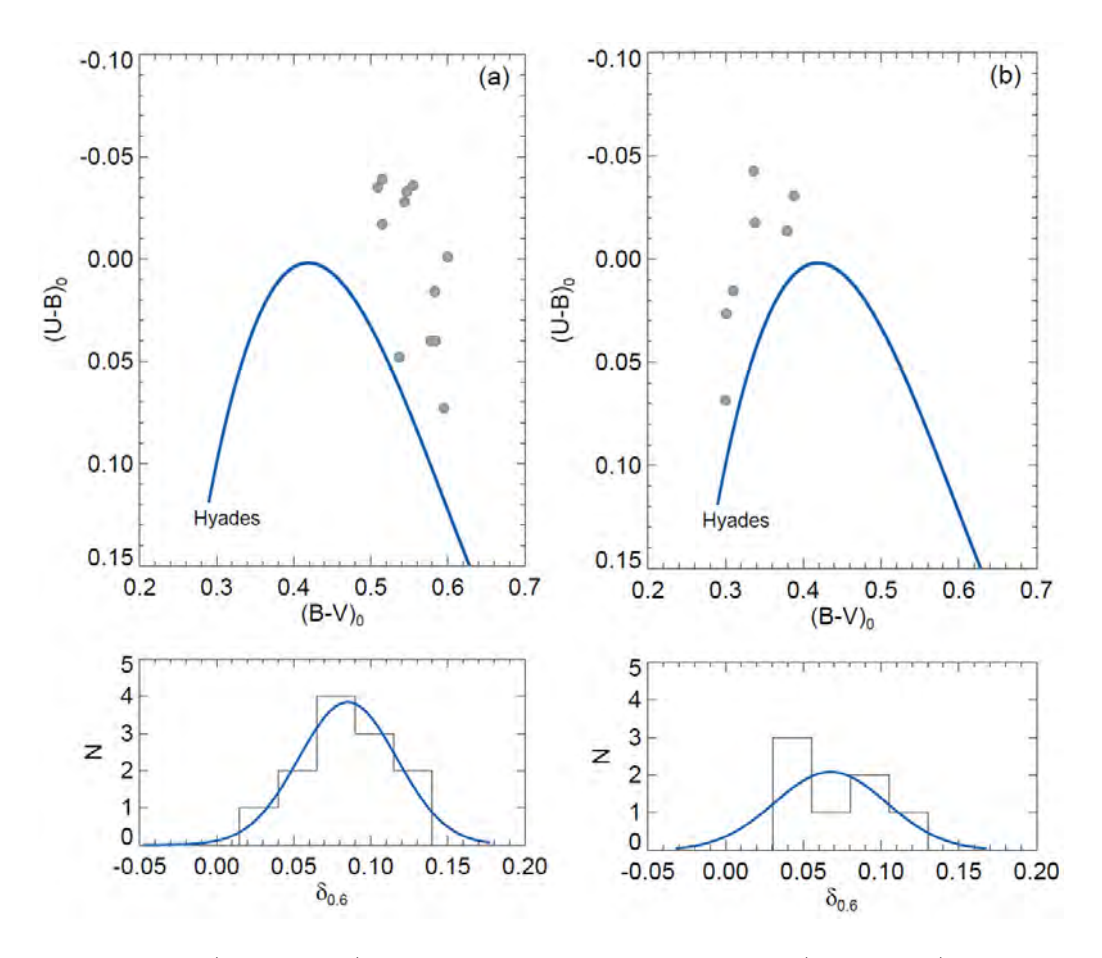


Fig. 8. Two-color diagrams (upper panels) and the distributions of normalised  $\delta_{0.6}$  (lower panels) for NGC 1193 (a) and NGC 1798 (b). The solid blue lines in the upper and lower panels represent the main-sequence of Hyades and Gaussian models which were fitted to the histograms, respectively. The color figure can be viewed online.

and  $d_{\rm iso} = 4451 \pm 728$  pc for NGC 1798. The  $V \times (U-B)$ ,  $V \times (B-V)$ , and  $G \times (G_{\rm BP}-G_{\rm RP})$  CMDs with the best fit isochrones and associated errors are shown in Figure 9.

The isochrone-based distance for NGC 1193 as estimated by this study is compatible with the result given by Tadross (2005,  $d=5.25\pm0.24$  kpc). As well, the estimated age of the cluster is in a good agreement with the value of Kyeong et al. (2008,  $t=5.0\pm1.3$  Gyr). For NGC 1798, the derived distance matches well within the errors with the result of Park & Lee (1999,  $d=4.2\pm0.3$  kpc). The age of the cluster is coherent with the findings given by Park & Lee (1999,  $t=1.4\pm0.2$  Gyr) and Maciejewski & Niedzielski (2007, t=1.6 Gyr).

Applying the linear equation of  $\varpi$  (mas) = 1000/d (pc), we converted isochrone distances to trigonometric parallaxes for the two clusters. This indicated that the parallax distances of NGC 1193 and NGC 1798 are  $\varpi_{\rm iso} = 0.180 \pm 0.012$  mas and  $\varpi_{\rm iso} = 0.225 \pm 0.037$  mas, respectively. It is con-

cluded that these values are in good agreement with the *Gaia* EDR3 trigonometric parallax distances for both clusters.

## 5. KINEMATICS AND GALACTIC ORBIT PARAMETERS OF CLUSTERS

The MWPOTENTIAL2014 (Bovy 2015) algorithm, one of the potential functions defined in GALPY (the galactic dynamics library, Bovy 2015<sup>10</sup>), was applied to calculate the space velocity components and galactic orbital parameters for NGC 1193 and NGC 1798. The algorithm assumes an axisymmetric potential for the Milky Way galaxy. We adopted the galactocentric distance to be  $R_{\rm GC}=8$  kpc, the Solar circular velocity of  $V_{\rm rot}=220~{\rm km~s^{-1}}$  (Bovy 2015; Bovy & Tremaine 2012), and the Solar distance from the galactic plane as  $27\pm4~{\rm pc}$  (Chen et al. 2000). Since the MWPoTENTIAL2014 code comprises bulge, disk, and halo

<sup>&</sup>lt;sup>10</sup>See also https://galpy.readthedocs.io/en/v1.5.0/

TABLE 3
METALLICITIES CALCULATED FOR TWO CLUSTERS. $N$ IS THE NUMBER OF MEMBER STARS
USED IN THE ANALYSES

		NGC 1193				NGC 1798	
$\langle [Fe/H] \rangle$ (dex)	N	Survey/Catalog/Telescope	Ref	$\langle [Fe/H] \rangle$ (dex)	N	Survey/Catalog/Telescope	Ref
$-0.51 \pm 0.09$	4	KPNO	(01)	$-0.18 \pm 0.02$	4	KPNO	(10)
$-0.22\pm0.14$	2	$\operatorname{HET}$	(02)	-0.165	4	KPNO	(11)
$-0.17\pm0.13$	1	$\operatorname{HET}$	(03)	$-0.18 \pm 0.01$	4	KPNO	(06)
$-0.22\pm0.01$	1	PASTEL	(04)	-0.294	4	KPNO	(12)
-0.17	1	$\operatorname{HET}$	(05)	$-0.34 \pm 0.01$	4	KPNO	(13)
$-0.25\pm0.01$	2	APOGEE DR14	(06)	$-0.200 \pm 0.006$	4	KPNO	(14)
$-0.34 \pm 0.01$	3	APOGEE DR16	(07)	$-0.30\pm0.02$	4	KPNO	(15)
$-0.320 \pm 0.012$	1	GALAH DR3	(08)	$-0.27\pm0.03$	4	KPNO	(07)
$-0.30 \pm 0.06$	12	SPMO	(09)	$-0.267 \pm 0.007$	4	KPNO	(08)
				$-0.20\pm0.07$	7	SPMO	(09)

(01) Friel et al. (2002), (02) Friel, Jacobson, & Pilachowski (2010), (03) Jacobson & Friel (2013), (04) Heiter et al. (2014), (05) Overbeek, Friel, & Jacobson (2016), (06) Carrera et al. (2019), (07) Donor et al. (2020), (08) Spina et al. (2021), (09) This study, (10) Donor et al. (2018), (11) Ting, Hawkins, & Rix (2018), (12) Ting & Rix (2019), (13) Hasselquist et al. (2020), (14) Sit & Ness (2020), (15) Olney et al. (2020).

potentials of the Milky Way, we assumed that it well represents the Galaxy.

Bovy (2015) defined the bulge component as a spherical power law density profile, given as follows:

$$\rho(r) = A \left(\frac{r_1}{r}\right)^{\alpha} \exp\left[-\left(\frac{r}{r_c}\right)^2\right],\tag{4}$$

where  $r_1$  is the present reference radius,  $r_c$  the cut-off radius, A the amplitude that is applied to the potential in mass density units, and  $\alpha$  is the inner power. We adopted the potential presented by Miyamoto & Nagai (1975) for the galactic disk component:

$$\Phi_{\rm disk}(R_{\rm GC}, Z) = -\frac{GM_{\rm d}}{\sqrt{R_{\rm GC}^2 + \left(a_{\rm d} + \sqrt{Z^2 + b_{\rm d}^2}\right)^2}}.$$
(5)

 $R_{\rm GC}$  is the distance from the galactic center, Z the vertical distance from the galactic plane, G the universal gravitational constant,  $M_{\rm d}$  the mass of the galactic disk, and  $a_{\rm d}$  and  $b_{\rm d}$  are the scale-length and scale-height of the disk, respectively.

The potential for the halo component was obtained by Navarro et al. (1996) as:

$$\Phi_{\rm halo}(r) = -\frac{GM_{\rm s}}{R_{\rm GC}} \ln \left( 1 + \frac{R_{\rm GC}}{r_{\rm s}} \right), \qquad (6)$$

where  $M_{\rm s}$  is the mass of the dark matter halo of the Milky Way and  $r_{\rm s}$  is its radius.

To determine the spacial velocities and galactic orbit parameters of NGC 1193 and NGC 1798, we used the equatorial coordinates, proper motion components, distances, and radial velocity data with their uncertainties in the calculations. These values are listed in Table 4. We performed kinematic and dynamic analyses with 1 Myr steps over a 3.5 Gyr integration time. We considered the proper motion components and distances of the two clusters as derived by this study (see § 3.3), while for the radial velocities we used the data of Donor et al. (2020) who gave  $\langle V_{\rm r} \rangle = -84.7 \pm 0.2$  km s<sup>-1</sup> for NGC 1193 and  $\langle V_{\rm r} \rangle = 2.7 \pm 0.8$  km s<sup>-1</sup> for NGC 1798. As a result, we obtained for both clusters estimates of apogalactic distance  $R_{\rm a}$ , perigalactic distance  $R_{\rm p}$ , eccentricity e, maximum vertical distance from galactic plane  $Z_{\text{max}}$ , galactic space velocity components (U, V, W), and orbital period T. These estimates are listed in Table 4. The space velocity components (U, V, W) were calculated as  $(70.95 \pm 0.16, -47.62 \pm 0.10, 5.56 \pm 0.59) \text{ km s}^{-1} \text{ for}$ NGC 1193 and  $(-7.18 \pm 1.50, -14.64 \pm 2.27, 9.13 \pm$ 1.69) km s<sup>-1</sup> for NGC 1798. In their study based on Gaia DR2 astrometric data (Gaia collaboration et al. 2018), Soubiran et al. (2018) derived the space velocity components for NGC 1193 as (U, V, W) = $(68.84 \pm 0.53, -46.77 \pm 0.54, 9.00 \pm 0.65) \text{ km s}^{-1}$ and for NGC 1798 as  $(U, V, W) = (7.50 \pm 0.41,$  $-16.63 \pm 0.50$ ,  $12.85 \pm 0.39$ ) km s<sup>-1</sup>. These results are in good agreement with the values cal-

TABLE 4	
FUNDAMENTAL PARAMETERS OF NGC 1193 AND NGC	1798

Parameter	NGC 1193	NGC 1798			
$(\alpha, \delta)_{\rm J2000}$ (Sexagesimal)	03:05:56.64, +44:22:58.80	05:11:39.36, +47:41:27.60			
$(l,b)_{\rm J2000}$ (Decimal)	146.8143, -12.1624	160.7043, +04.8500			
$f_0$ (stars arcmin <sup>-2</sup> )	$166.865 \pm 1.573$	$53.597 \pm 3.789$			
$r_{\rm c}$ (arcmin)	$0.526 \pm 0.009$	$1.190 \pm 0.057$			
$f_{\rm bg}  ({\rm stars  arcmin^{-2}})$	$5.225 \pm 0.124$	$11.318 \pm 0.321$			
$r_{ m lim}$ (arcmin)	8	8			
r (pc)	12.95	10.36			
$\mu_{\alpha}\cos\delta$ (mas yr <sup>-1</sup> )	$-0.207 \pm 0.009$	$0.793 \pm 0.006$			
$\mu_{\delta} \; (\text{mas yr}^{-1})$	$-0.431 \pm 0.008$	$-0.373 \pm 0.005$			
Cluster members $(P \ge 0.5)$	181	161			
$\varpi$ (mas)	$0.191 \pm 0.157$	$0.203 \pm 0.099$			
E(B-V) (mag)	$0.150 \pm 0.037$	$0.505 \pm 0.100$			
E(U-B) (mag)	$0.109 \pm 0.027$	$0.376 \pm 0.073$			
$A_{ m V} \ ({ m mag})$	$0.465 \pm 0.084$	$1.566 \pm 0.310$			
[Fe/H] (dex)	$-0.30 \pm 0.06$	$-0.20 \pm 0.07$			
Age (Gyr)	$4.6 \pm 1.0$	$1.3 \pm 0.2$			
Distance modulus (mag)	$14.191 \pm 0.149$	$14.808 \pm 0.332$			
Isochrone distance (pc)	$5562 \pm 381$	$4451 \pm 728$			
$(X,Y,Z)_{\odot}$ (pc)	(-4550, 2976, 1172)	(-4186, 1466, 376)			
$R_{\mathrm{GC}} \; (\mathrm{kpc})$	12.90	12.27			
PDMF slope	$-1.38 \pm 2.16$	$-1.30 \pm 0.21$			
$U_{\rm LSR}~({\rm km/s})$	$79.78 \pm 0.29$	$1.65 \pm 1.51$			
$V_{ m LSR}~({ m km/s})$	$-33.43 \pm 0.35$	$-0.45 \pm 2.30$			
$W_{ m LSR}~({ m km/s})$	$12.13 \pm 0.62$	$15.70 \pm 1.70$			
$S_{ m LSR}$ (km/s)	$87.35 \pm 0.77$	$15.79 \pm 3.23$			
$R_{\rm a}~({ m kpc})$	$14.44 \pm 0.34$	$14.11 \pm 0.30$			
$R_{ m p} \; ({ m kpc})$	$10.80 \pm 0.43$	$11.72 \pm 0.50$			
$z_{ m max}~( m pc)$	$1342 \pm 77$	$725 \pm 148$			
e	$0.144 \pm 0.008$	$0.092 \pm 0.011$			
$T  ext{ (Myr)}$	$370 \pm 12$	$381 \pm 23$			
Birthplace (kpc)	10.86	11.82			

culated in the study. The correction to the local standard of rest (LSR), given by Coşkunoğlu et al. (2011) as  $(U,V,W)=(8.83\pm0.24,\ 14.19\pm0.34,\ 6.57\pm0.21)\ {\rm km\ s^{-1}}$ , was applied to the space velocity components. The derived LSR corrected space velocity components are  $(U,V,W)_{\rm LSR}=(79.78\pm0.29,\ -33.43\pm0.35,\ 12.13\pm0.62)\ {\rm km\ s^{-1}}$  for NGC 1193 and  $(U,V,W)_{\rm LSR}=(1.65\pm1.51,\ -0.45\pm2.30,\ 15.70\pm1.70)\ {\rm km\ s^{-1}}$  for NGC 1798. Moreover, the space velocities of NGC 1193 were calculated to be 87.35  $\pm$  0.77 km s<sup>-1</sup> and 15.79  $\pm$  3.23 km s<sup>-1</sup> for NGC 1798.

Considering the space velocity components of stars in different Galactic populations, Schuster et al. (2012) divided the stars into thin disk ( $-50 < V_{\rm LSR}$  km/s), thick disk ( $-180 < V_{\rm LSR} \le -50$  km/s) and halo ( $V_{\rm LSR} \le 180$  km/s) groups. Figure 10 shows the positions of the clusters according to the Schuster et al. (2012)'s kinematic criteria. According to these criteria, the open clusters NGC 1193

and NGC 1798 appear to be members of the thick disk and thin disk populations, respectively. Considering the metal abundance range of NGC 1193 ( $-0.51 \leq [{\rm Fe/H}] \leq -0.17$  dex, see Table 3), it is concluded that the cluster belongs to the metal-rich side of the thick-disk population.

Figure 11 presents the orbits of NGC 1193 (Figure 11a) and NGC 1798 (Figure 11c) as functions of distance from the galactic center and the galactic plane ( $Z \times R_{\rm GC}$  and  $R_{\rm GC} \times t$ ). The birth and present-day locations for the two clusters are marked with yellow triangles and circles in sub-figures 11b and 11d. Figures 11a and 11c show that both of the clusters entirely orbit outside the solar circle. The orbital eccentricities of NGC 1193 and NGC 1798 are smaller than 0.15, thus their orbits are close to circular. The results of orbital integrations imply that NGC 1193 reaches its maximum vertical distance from the galactic plane at  $Z_{\rm max} = 1342 \pm 77$  pc

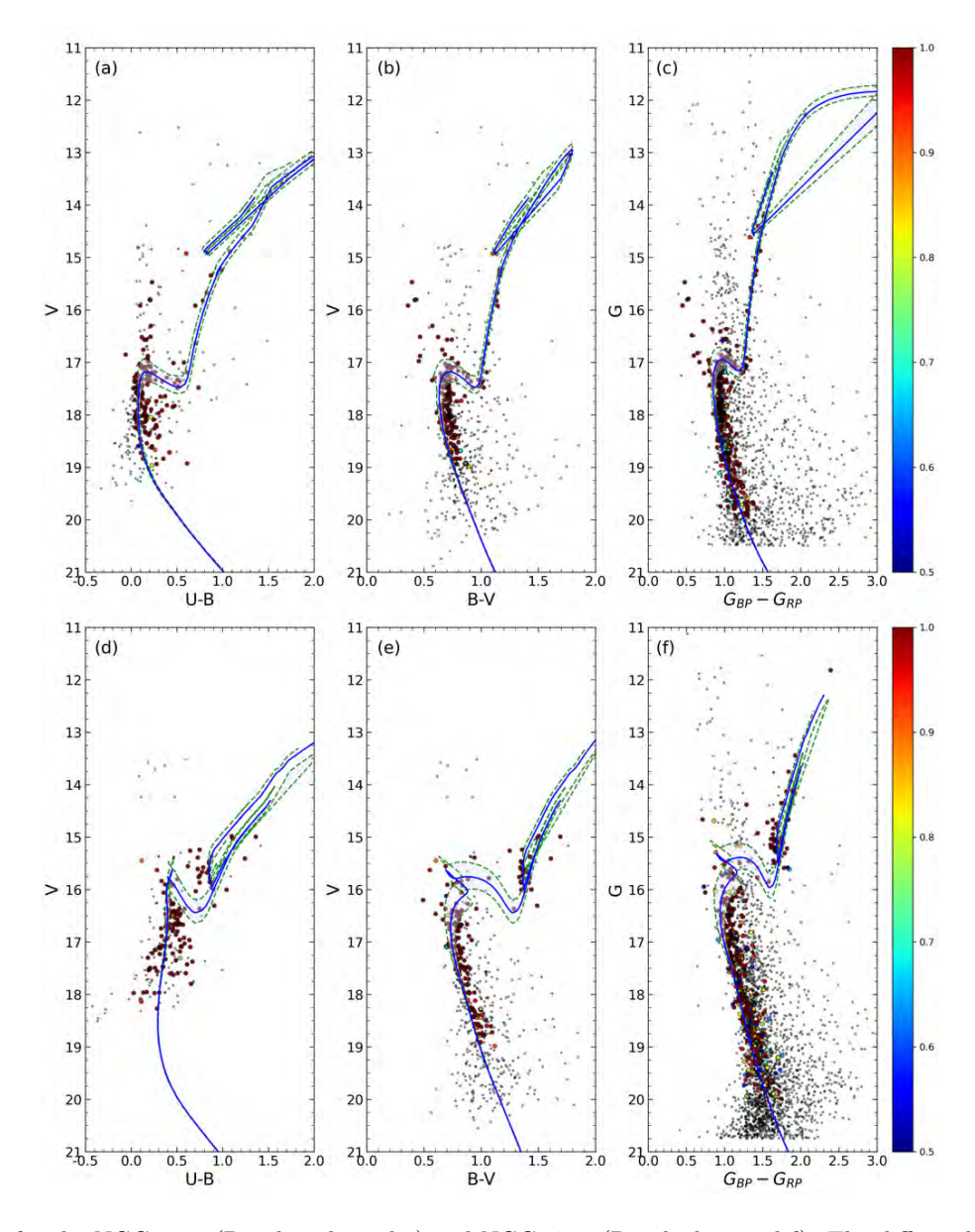


Fig. 9. CMDs for the NGC 1193 (Panels a, b, and c) and NGC 1798 (Panels d, e, and f). The differently colored dots represent the membership probabilities according to the color scales shown on the right side of the diagrams. Grey dots indicate low probability members (P < 0.5), or field stars (P = 0). The blue lines show the PARSEC isochrones, while the shaded areas surrounding these lines are their associated errors. The color figure can be viewed online.

with an orbital period  $T=370\pm12$  Myr, and these values correspond to  $Z_{\rm max}=725\pm148$  pc and  $T=381\pm23$  Myr for NGC 1798. Considering the age values determined in this study for the clusters, we ran the GALPY program backwards in time and examined the resulting birth–places. The program indicated that the birth-place radial distances are 10.86 kpc and 11.82 kpc for NGC 1193 and NGC 1798, respectively, meaning that the clusters were born in the metal-poor region outside the solar circle.

## 6. LUMINOSITY AND PRESENT-DAY MASS FUNCTIONS

The distribution of stars according to their brightness is defined as the luminosity function (LF). We used Gaia EDR3 photometric data to determine LFs for the two clusters. For this, main-sequence stars located inside the 8 arcmin limiting radii, as derived above, were selected for the two clusters. The magnitude ranges of the chosen stars are within the  $17.25 \leq G \leq 20$  mag for NGC 1193 and  $16.5 \leq G \leq 20$  mag for NGC 1798. We converted the G magnitude ranges of the chosen stars are within the

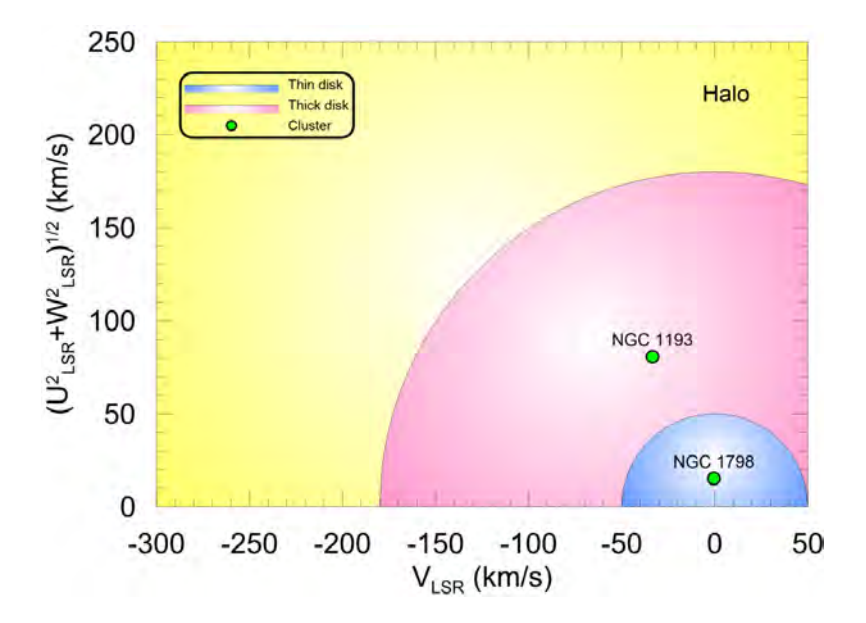


Fig. 10. Toomre diagram for NGC 1193 and NGC 1798. Blue, pink and yellow regions show thin disk, thick disk and halo populations, respectively. The color figure can be viewed online.

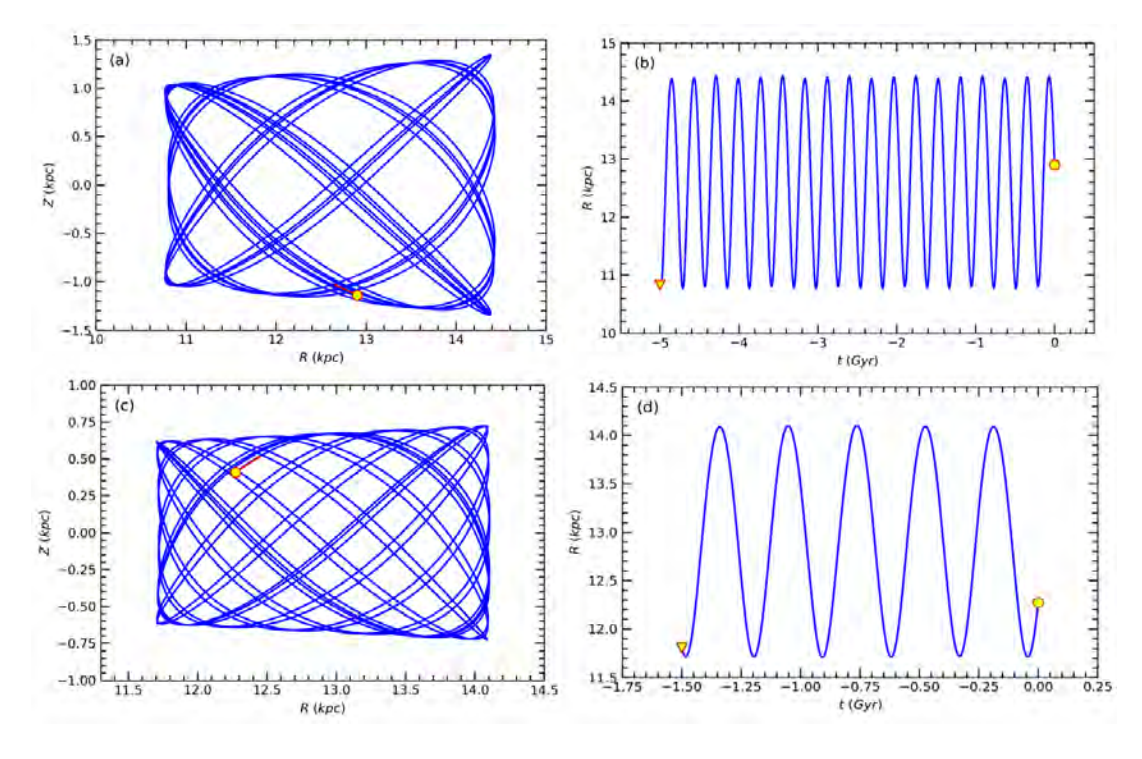


Fig. 11. The galactic orbits and birth radii of NGC 1193 (a,b) and NGC 1798 (c,d) in the  $Z \times R_{\rm GC}$  and  $R_{\rm GC} \times t$  planes. The filled yellow circles and triangles show the present day and birth positions, respectively. Red arrows are the motion vectors of OCs. The color figure can be viewed online.

nitudes of the selected stars to absolute magnitudes with the equation  $M_{\rm G} = G - 5 \times \log d + 5 + A_{\rm G}$ , where G is the apparent magnitude and d the distance derived earlier in this study.  $A_G$  is the extinction for G

magnitudes and is represented by  $A_G = 0.84 \times A_V$  (Sun et al. 2021) (here  $A_V$  is the extinction for V magnitudes). This led to the absolute magnitude ranges being limited within the  $2.5 < M_{\rm G} < 5.5$  and

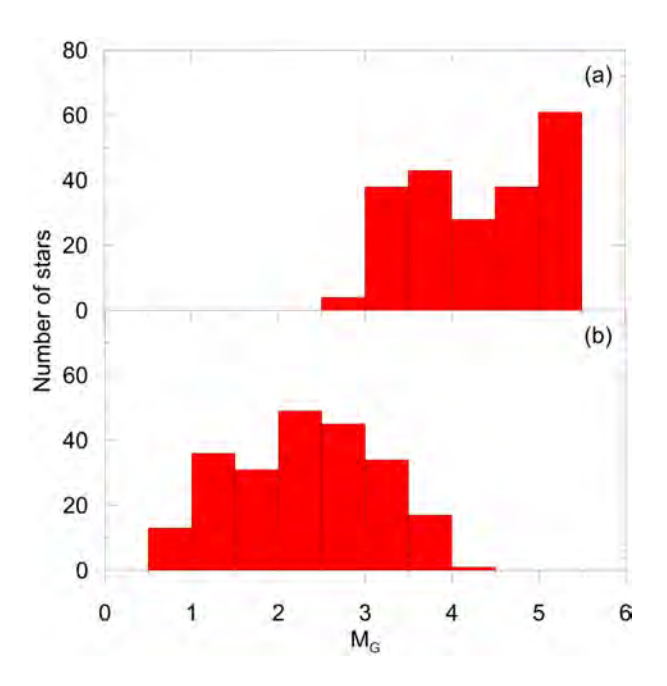


Fig. 12. The luminosity functions of NGC 1193 (a) and NGC 1798 (b). The histograms show the absolute magnitudes of the main-sequence stars belonging to the clusters. The color figure can be viewed online.

 $0.5 < M_{\rm G} < 4.5$  mag for NGC 1193 and NGC 1798, respectively. We constructed LF histograms with the step-size 0.5 mag, as shown as Figure 12 for both clusters.

To convert these LFs to present day mass functions (PDMFs) we employed the PARSEC isochrones (Bressan et al. 2012), which give the ages and metal abundances (z) of the clusters. We utilized a high degree polynomial equation between G-band absolute magnitudes and masses of theoretical main-sequence stars. The resulting absolute magnitude-mass relation was used to transform the observational absolute G band magnitudes to masses. The number, mass range, and mean mass of main-sequence stars that resulted are 212,  $0.85 \leq M/M_{\odot} \leq 1.2$ , and  $0.99M_{\odot}$  for NGC 1193, and 226,  $1.1 \leq M/M_{\odot} \leq 2$ , and  $1.53~M_{\odot}$  for NGC 1798. The mass function PDMF can be approximated by a power law defined as by Salpeter (1955):

$$\log(\frac{dN}{dM}) = -(1+\Gamma) \times \log(M) + \text{constant.}$$
 (7)

Here dN is the number of stars in a mass bin of width dM with a central mass M and  $\Gamma$  being the slope of the PDMF. We estimated the slope of the PDMF in both clusters for apparent  $G \leq 20$  mag, which

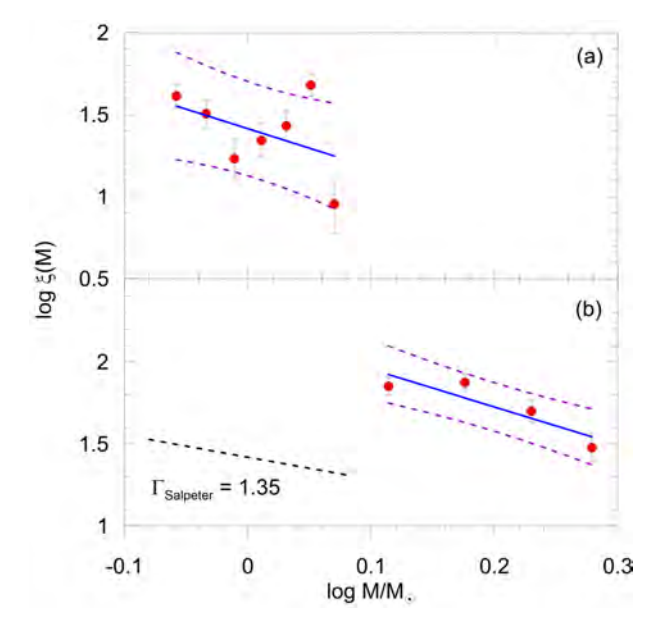


Fig. 13. Present-day mass functions of NGC 1193 (a) and NGC 1798 (b) derived from all samples (red circle). The blue and dashed lines represent the mass functions of the open clusters and Salpeter (1955)'s mass function, respectively. The purple dashed lines show  $\pm 1\sigma$  prediction levels. The color figure can be viewed online.

corresponds to stars more massive than  $0.85\,M_\odot$  in NGC 1193 and  $1.1 M_{\odot}$  for NGC 1798. The resulting PDMFs with the best fits are presented in Figure 13. We calculated the slope values to be  $\Gamma = 1.38 \pm 2.16$ for NGC 1193 and as  $\Gamma = 1.30 \pm 0.21$  for NGC 1798. Since the NGC 1193 cluster is about 5.5 kpc from the Sun, the magnitudes of the main-sequence stars are within a narrow range. This causes the mass range of the main-sequence stars to be limited and the distribution of the mass function to show a large scatter. While the PDMF of the NGC 1193 is compatible with Salpeter (1955)'s result of  $\Gamma = 1.35$ , the error of the PDMF is large. This situation is different for NGC 1798. Considering the value and error of the PDMF for NGC 1798, it is in agreement with Salpeter's result.

#### 7. SUMMARY AND CONCLUSION

We performed photometric, astrometric, and kinematic studies of two old age open clusters, NGC 1193 and NGC 1798, using CCD UBV and Gaia EDR3 data. We examined the cluster structure, obtaining basic astrophysical parameters as well as properties of galactic orbits for two clusters. Outcomes of the study are listed in Table 4 and summarised as follows:

- 1. Performing the RDP analyses, we determined the limiting radii  $r_{\rm lim}=8$  arcmin for both clusters. This value corresponds to limiting radii of 12.95 pc and 10.36 pc for NGC 1193 and NGC 1798, respectively. We considered the stars within these limiting radii as potential cluster members and restricted subsequent analysis to this set of stars.
- 2. The calculation of membership probabilities of stars was made using the UPMASK program together with a five-dimensional parameter space containing the stars' proper motion components, trigonometric parallaxes, and their uncertainties. We considered the stars with probabilities  $P \geq 0.5$  to be cluster members. Additionally we adopted two more criteria to clarify cluster membership:
  - (a) binary star contamination in the cluster main-sequences which was interpreted by the de-reddened ZAMS fitted to  $V \times (B-V)$  CMDs with a shift of +0.75 mag in the V band, and
  - (b) within the limiting radii determined in the study (as per step 1).

Consequently, we selected the stars inside the clusters' limiting radii, within best-fitting ZAMS and with the membership probability  $P \geq 0.5$  as 'real' members of two clusters. Thus we identified 361 and 428 stars as most likely members of NGC 1193 and NGC 1798, respectively.

- 3. The reddening and photometric metallicities of the two clusters were derived separately using CCD *UBV* TCDs. The reddening analyses were performed by fitting de-reddened ZAMS to main sequence member stars. Photometric metallicity was based on the comparison of F-G type main sequence members with the Hyades main-sequence. reddening and photometric metallicity for NGC 1193 are  $E(B-V) = 0.150 \pm 0.037$  mag and  $[Fe/H] = -0.30 \pm 0.06$  dex, respectively. The corresponding values for NGC  $E(B-V) = 0.505 \pm 0.100 \text{ mag}$ are and  $[Fe/H] = -0.20 \pm 0.07 \text{ dex.}$
- 4. The distance moduli, distance, and age of the NGC 1193 were derived as  $\mu_{\rm V}=14.191\pm0.149$  mag,  $d=5562\pm381$  pc, and  $t=4.6\pm1$  Gyr, respectively. Similarly

- $\mu_{\rm V}=14.808\pm0.332$  mag,  $d=4451\pm728$  pc, and  $t=1.3\pm0.2$  Gyr were calculated for NGC 1798. These results were obtained by simultaneously fitting PARSEC isochrones on the UBV and Gaia EDR3 photometric CMDs utilizing the most likely member stars according to reddening and metallicities derived in the study.
- 5. Mean proper motion components were calculated as  $(\mu_{\alpha}\cos\delta, \mu_{\delta}) = (-0.207 \pm 0.009, -0.431 \pm 0.008)$  mas yr<sup>-1</sup> for NGC 1193 as well as  $(\mu_{\alpha}\cos\delta, \mu_{\delta}) = (0.793 \pm 0.006, -0.373 \pm 0.005)$  mas yr<sup>-1</sup> for NGC 1798.
- 6. We estimated mean trigonometric parallaxes using Gaia EDR3 data of most likely members for two clusters. The results are  $\varpi_{\mathrm{Gaia}} = 0.191 \pm 0.157 \; \mathrm{mas} \; \mathrm{for} \; \mathrm{NGC} \; 1193 \; \mathrm{and}$  $\varpi_{\rm Gaia} = 0.203 \pm 0.099 \text{ mas for NGC 1798. We}$ also converted isochrones distances to trigonometric parallaxes by applying the linear equation  $\varpi$  (mas) = 1000/d (pc) and found  $\varpi_{iso}$  =  $0.180 \pm 0.012$  mas for NGC 1193 and  $\varpi_{\rm iso}$  =  $0.225 \pm 0.037$  mas for NGC 1798. For both clusters our derived trigonometric parallaxes values calculated from isochrone fitting distances are well supported by the values determined from Gaia EDR3 trigonometric parallaxes of member stars.
- 7. Space velocities and galactic orbital parameters show that NGC 1193 belongs to the thick-disk population, whereas NGC 1798 is a member of the thin-disk population. Moreover, both clusters orbit completely outside the solar circle.
- 8. We found that NGC 1193 and NGC 1798 were born outside the solar circle with the birth radii of 10.86 and 11.82 kpc from the Galactic center, respectively. These birth radii indicate the metal-poor formation region and support the metallicities calculated in the study for the two clusters.
- 9. Present day function slopes of mass  $\Gamma = 1.38 \pm 2.16$  and  $\Gamma = 1.30 \pm 0.21$  were derived for NGC 1193 and NGC 1798, respectively. While the results for two clusters are in good agreement with the value of Salpeter (1955), that for NGC 1193 possesses a large uncertainty. We concluded that because of its distance, the main-sequence stars of NGC 1193 are limited within a narrow range of magnitudes.

The observations of this publication were made at the National Astronomical Observatory, San Pedro Mártir, Baja California, México, and the authors wish to thank the staff of the Observatory for their assistance during these observations. This research has made use of the WEBDA database, operated at the Department of Theoretical Physics and Astrophysics of the Masaryk University. This research has made use of NASA's Astrophysics Data System. We also made use of VizieR and Simbad databases at CDS, Strasbourg, France as well as data from the European Space Agency (ESA) mission Gaia<sup>11</sup>, processed by the Gaia Data Processing and Analysis Consortium (DPAC)<sup>12</sup>. Funding for DPAC has been provided by national institutions, in particular the institutions participating in the Gaia Multilateral Agreement. IRAF was distributed by the National Optical Astronomy Observatory, which was operated by the Association of Universities for Research in Astronomy (AURA) under a cooperative agreement with the National Science Foundation. PyRAF is a product of the Space Telescope Science Institute, which is operated by AURA for NASA. We thank the University of Queensland for collaboration software.

#### REFERENCES

- Ahumada, J. A. & Lapasset, E. 2007, A&A, 463, 789, https://doi.org/10.1051/0004-6361:20054590
- Ak, T., Bostanci, Z. F., Yontan, T., et al. 2016, Ap&SS, 361, 126, https://doi.org/10.1007/s10509-016-2707-2
- Akbulut, B., Ak, S., Yontan, T., et al. 2021, Ap&SS, 366, 68, https://doi.org/10.1007/ s10509-021-03975-x
- Banks, T., Yontan, T., Bilir, S. & Canbay, R. 2020, JApA, 41, 6, https://doi.org/10.1007/s12036-020-9621-2
- Bertelli, G., Bressan, A., Chiosi, C., Fagotto, F. & Nasi, E. 1994, A&AS, 106, 275
- Bressan, A., Marigo, P., Girardi, L., et al. 2012, MNRAS, 427, 127, https://doi.org/10.1111/j.1365-2966. 2012.21948.x
- Bilir, S., Güver, T. & Aslan, M. 2006, AN, 327, 693, https://doi.org/10.1002/asna.200510614
- Bilir, S., Güver, T., Khamitov, I., Ak, T., Ak, S., Coşkunoğlu, K. B., Paunzen, E. & Yaz, E. 2010, Ap&SS, 326, 139, https://doi.org/10.1007/ s10509-009-0233-1
- Bilir, S., Bostancı, Z. F., Yontan, T., et al. 2016, Ad-SpR, 58, 1900, https://doi.org/10.1016/j.asr. 2016.06.039
- Bostancı, Z. F., Ak, T., Yontan, T., et al. 2015, MN-RAS, 453, 1095, https://doi.org/10.1093/mnras/stv1665
  - <sup>11</sup>https://www.cosmos.esa.int/gaia
  - $^{12} \rm https://www.cosmos.esa.int/web/gaia/dpac/consortium$

- Bostanci, Z. F., Yontan, T., Bilir, S., et al. 2018, Ap&SS, 363, 143, https://doi.org/10.1007/ s10509-018-3364-4
- Bovy, J. & Tremaine, S. 2012, ApJ, 756, 89, https://doi.org/10.1088/0004-637X/756/1/89
- Bovy, J. 2015, ApJS, 216, 29, https://doi.org/10. 1088/0067-0049/216/2/29
- Cantat-Gaudin, T., Jordi, C., Vallenari, A., et al. 2018, A&A, 618, 93, https://doi.org/10.1051/ 0004-6361/201833476
- Cantat-Gaudin, T., Anders, F., Castro-Ginard, A., et al. 2020, A&A, 640, 1, https://doi.org/10.1051/ 0004-6361/202038192
- Carraro, G., Sales Silva, J. V., Moni Bidin, C. & Vazquez, R. A. 2017, ApJ, 153, 99, https://doi.org/10. 3847/1538-3881/153/3/99
- Carrera, R. 2012, A&A, 544, 109, https://doi.org/10. 1051/0004-6361/201219625
- Carrera, R., Bragaglia, A., Cantat-Gaudin, T., et al. 2019, A&A, 623, 80, https://doi.org/10.1051/ 0004-6361/201834546
- Chen, Y. Q., Nissen, P. E., Zhao, G., Zhang, H. W. & Benoni, T. 2000, A&AS, 141, 491, https://doi.org/ 10.1051/aas:2000124
- Conrad, C., Scholz, R.-D., Kharchenko, N. V., et al. 2014, A&A, 562, 54, https://doi.org/10.1051/ 0004-6361/201322070
- Coşkunoğlu, B., Ak S., Bilir, S., et al. 2011, MNRAS, 412, 1237, https://doi.org/10.1111/j.1365-2966. 2010.17983.x
- Donor, J., Frinchaboy, P. M., Cunha, K., et al. 2018, AJ, 156, 142, https://doi.org/10.3847/ 1538-3881/aad635
- Donor, J., Frinchaboy, P. M., Cunha, K., et al. 2020, AJ, 159, 199, https://doi.org/10.3847/ 1538-3881/ab77bc
- Dreyer, J. L. E. 1888, MmRAS, 49, 1
- Eker, Z., Bakış, V., Bilir, S., et al. 2018, MNRAS, 479, 5491, https://doi.org/10.1093/mnras/sty1834
- Eker, Z., Soydugan, F., Bilir, S., et al. 2020, MN-RAS, 496, 3887, https://doi.org/10.1093/mnras/staa1659
- Friel, E. D., Liu, T. & Janes, K. A. 1989, PASP, 101, 1105, https://doi.org/10.1086/132583
- Friel, E. D. & Janes, K. A. 1993, A&A, 267, 75
- Friel, E. D. 1995, ARA&A, 33, 381, https://doi.org/ 10.1146/annurev.aa.33.090195.002121
- Friel, E. D., Janes, K. A., Tavarez, M., et al. 2002, AJ, 124, 2693, https://doi.org/10.1086/344161
- Friel, E. D., Jacobson, H. R. & Pilachowski, C. A. 2010, AJ, 139, 1942, https://doi.org/10.1088/ 0004-6256/139/5/1942
- Gaia Collaboration, Prusti, T., de Bruijne, J. H. J. et al. 2016, A&A, 595, 1, https://doi.org/10.1051/ 0004-6361/201629272
- Gaia Collaboration, Brown, A. G. A., Vallenari, A., Prusti, T., et al. 2018, A&A, 616, 1, https://doi.org/10.1051/0004-6361/201833051

- Gaia Collaboration, Brown, A. G. A., Vallenari, A., Prusti, T., et al. 2021, A&A, 649, 1, https://doi. org/10.1051/0004-6361/202039657
- Garcia, B., Claria, J. J. & Levato, H. 1988, Ap&SS, 143, 317, https://doi.org/10.1007/BF00637143
- Gilmore, G., Randich, S., Asplund, M., et al. 2012, Msngr, 147, 25
- Hasselquist, S., Zasowski, G., Feuillet, D. K., et al. 2020, ApJ, 901, 109, https://doi.org/10.3847/ 1538-4357/abaeee
- Heiter, U., Soubiran, C., Netopil, M. & Paunzen, E. 2014, A&A, 561, 93, https://doi.org/10.1051/ 0004-6361/201322559
- Jacobson, H. R. & Friel, E. D. 2013, AJ, 145, 107, https: //doi.org/10.1088/0004-6256/145/4/107
- Janes, K. & Adler, D. 1982, ApJS, 49, 425, https://
  doi.org/10.1086/190805
- Janes, K. A. & Phelps, R. L. 1994, AJ, 108, 1773, https: //doi.org/10.1086/117192
- Kaluzny, J. 1988, AcA, 38, 339
- Karaali, S., Bilir, S., Karataş, Y. & Ak, S. G. 2003a, PASA, 20, 165, https://doi.org/10.1071/AS02028
- Karaali, S., Ak, S. G., Bilir, S., Karataş, Y. & Gilmore, G. 2003b, MNRAS, 343, 1013, https://doi.org/10. 1046/j.1365-8711.2003.06743.x
- Karaali, S., Bilir, S., Ak, S., Yaz, E. & Coşkunoğlu, B. 2011, PASA, 28, 95, https://doi.org/10.1071/ AS10026
- King, I. 1962, AJ, 67, 471, https://doi.org/10.1086/ 108756
- Koç, S., Yontan, T., Bilir, S., et al. 2022, AJ, 163, 191, https://doi.org/10.3847/1538-3881/ac58a0
- Kos, J., de Silva, G., Buder, S., et al. 2018, MNRAS, 480, 5242, https://doi.org/10.1093/mnras/sty2171
- Krone-Martins, A. & Moitinho, A. 2014, A&A, 561, 57, https://doi.org/10.1051/0004-6361/201321143
- Kyeong, J., Kim, S. C., Hiriart, D. & Sung, E.-C. 2008, JKAS, 41, 147, https://doi.org/10.5303/ JKAS.2008.41.6.147
- Landolt, A. U. 2009, AJ, 137, 4186, https://doi.org/ 10.1088/0004-6256/137/5/4186
- Lata, S., Pandey, A. K., Sagar, R. & Mohan, V. 2002, A&A, 388, 158, https://doi.org/10.1051/ 0004-6361:20020450
- Liu, L. & Pang, X. 2019, ApJS, 245, 32, https://doi. org/10.3847/1538-4365/ab530a
- Maciejewski, G. & Niedzielski, A. 2007, A&A, 467, 1065, https://doi.org/10.1051/0004-6361:20066588
- Miyamoto, M. & Nagai, R. 1975, PASJ, 27, 533
- Monet, D. G., Levine, S. E., Canzian, B., et al. 2003, AJ, 125, 984, https://doi.org/10.1086/345888

- Navarro, J. F., Frenk, C. S. & White, S. D. M. 1996, ApJ, 462, 563, https://doi.org/10.1086/177173
- Olney, R., Kounkel, M., Schillinger, C., et al. 2020, AJ, 159, 182, https://doi.org/10.3847/1538-3881/ab7a97
- Oralhan, İ. A., Karataş, Y., Schuster, W. J., Michel, R. & Chavarría, C. 2015, NewA, 34, 195, https://doi.org/10.1016/j.newast.2014.06.011
- Overbeek, J. C., Friel, E. D. & Jacobson, H. R. 2016, ApJ, 824, 75, https://doi.org/10.3847/0004-637X/824/2/75
- Park, H. S. & Lee, M. G. 1999, MNRAS, 304, 883, https://doi.org/10.1046/j.1365-8711.1999.02366.x
- Ruprecht, J. 1966, BAICz, 17, 33
- Salpeter, E. E. 1955, ApJ, 121, 161, https://doi.org/ 10.1086/145971
- Schuster, W. J., Moreno, E., Nissen, P. E. & Pichardo, B. 2012, A&A, 538, 21, https://doi.org/10.1051/ 0004-6361/201118035
- Sit, T. & Ness, M. K. 2020, ApJ, 900, 4, https://doi. org/10.3847/1538-4357/ab9ff6
- Soubiran, C., Cantat-Gaudin, T., Romero-Gómez, M., et al. 2018, A&A, 619, 155, https://doi.org/10.1051/0004-6361/201834020
- Spina, L., Ting, Y.-S., De Silva, G. M., et al. 2021, MN-RAS, 503, 3279, https://doi.org/10.1093/mnras/stab471
- Stetson, P. B. 1987, PASP, 99, 191, https://doi.org/ 10.1086/131977
- Stetson, P. B., Pancino, E., Zocchi, A., Sanna, N. & Monelli, M. 2019, MNRAS, 485, 3042, https://doi.org/10.1093/mnras/stz585
- Sun, M., Jiang, B., Yuan, H. & Li, J. 2021, ApJS, 254, 38, https://doi.org/10.3847/1538-4365/abf929
- Sung, H., Lim, B., Bessell, M. S., et al. 2013, JKAS, 46, 103, https://doi.org/10.5303/JKAS.2013.46. 3.103
- Tadross, A. L. 2005, AN, 326, 19, https://doi.org/10. 1002/asna.200410335
- Ting, Y.-S., Hawkins, K. & Rix, H.-W. 2018, ApJL, 858, 7, https://doi.org/10.3847/2041-8213/aabf8e
- Ting, Y.-S. & Rix, H.-W. 2019, ApJ, 878, 2, https://
  doi.org/10.3847/1538-4357/ab1ea5
- van den Bergh, S. & Sher, D. 1960, PDDO, 2, 203
- Yontan, T., Bilir, S., Bostancı, Z. F., et al. 2015, Ap&SS, 355, 267, https://doi.org/10.1007/ s10509-014-2175-5
- Yontan, T., Bilir, S., Bostancı, Z. F., et al. 2019, Ap&SS, 364, 152, https://doi.org/10.1007/ s10509-019-3640-y
- Yontan, T., Bilir, S., Ak, T., et al. 2021, AN, 342, 538, https://doi.org/10.1002/asna.202113837

- Talar Yontan, Hikmet Çakmak & Selçuk Bilir: Istanbul University, Faculty of Science, Department of Astronomy and Space Sciences, 34119, Beyazıt, Istanbul, Turkey (talar.yontan@istanbul.edu.tr, hcakmak@istanbul.edu.tr, sbilir@istanbul.edu.tr).
- Timothy Banks: Nielsen, 200 W Jackson Blvd, Chicago, IL 60606, USA (tim.banks@nielsen.com); Department of Physical Science & Engineering, Harper College, 1200 W Algonquin Rd, Palatine, IL 60067, USA (tbanks@harpercollege.edu).
- Michel Raúl: Observatorio Astronomico Naciona, Universidad Nacional Autonoma de Mexico, Ensenada, Mexico (rmm@astro.unam.mx).
- Remziye Canbay, Seliz Koç, Seval Taşdemir, Hülya Erçay, Burçin Tanık Öztürk, & Deniz Cennet Dursun: Istanbul University, Institute of Graduate Studies in Science, Programme of Astronomy and Space Sciences, 34116, Beyazıt, Istanbul, Turkey (rmzycnby@gmail.com, seliskoc@gmail.com, tasdemir.seval@ogr.iu.edu.tr, hulyaercay5@gmail.com, burcin.tanik@istanbul.edu.tr, denizcdursun@gmail.com).